Published in final edited form as:
Nat Cell Biol. 2015 November ; 17(11): 1422–1434. doi:10.1038/ncb3241.

Complementary activities of TPX2 and chTOG constitute an efficient importin-regulated microtubule nucleation module

Johanna Roostalu[1], **Nicholas I. Cade**, and **Thomas Surrey**
The Francis Crick Institute, 44 Lincoln's Inn Fields, London WC2A 3LY, United Kingdom

Abstract

Spindle assembly and function require precise control of microtubule nucleation and dynamics. The chromatin-driven spindle assembly pathway exerts such control locally in the vicinity of chromosomes. One of the key targets of this pathway is TPX2. The molecular mechanism of how TPX2 stimulates microtubule nucleation is not understood. Using microscopy-based dynamic in vitro reconstitution assays with purified proteins, we find that human TPX2 directly stabilises growing microtubule ends and stimulates microtubule nucleation by stabilising early microtubule nucleation intermediates. Human microtubule polymerase chTOG (XMAP215/Msps/Stu2p/Dis1/Alp14 homolog) only weakly promotes nucleation, but acts synergistically with TPX2. Hence, a combination of distinct and complementary activities is sufficient for efficient microtubule formation in vitro. Importins control the efficiency of the microtubule nucleation by selectively blocking TPX2's interaction with microtubule nucleation intermediates. This in vitro reconstitution reveals the molecular mechanism of regulated microtubule formation by a minimal nucleation module essential for chromatin-dependent microtubule nucleation in cells.

The mitotic spindle ensures faithful chromosome segregation during cell division. In animal cells, spindles consist of a large number of microtubules and associated proteins[1]. Spindle function requires tight control of microtubule nucleation and dynamics.

One protein that contributes to controlling microtubule mass in spindles is XMAP215 from *Xenopus laevis*[2]. In vitro, purified XMAP215 acts as a microtubule polymerase by accelerating the addition of tubulin subunits to growing microtubule plus ends[3]. In *Xenopus* egg extract (XEE), absence of XMAP215 dramatically reduces microtubule mass, causing severe spindle defects[4, 5]. chTOG, the human homolog of XMAP215, has not been biochemically characterised yet. Its role in human cells appears to be less critical for proper spindle morphology as its depletion leads only to a moderate decrease in spindle length and microtubule density[6, 7] raising the question whether the activities of chTOG and XMAP215 are conserved.

[1] johanna.roostalu@crick.ac.uk.

AUTHOR CONTRIBUTIONS
J.R. and T.S. designed the study, J.R. generated the reagents and performed the experiments, J.R. and N.I.C. analysed the data, J.R. and T.S. wrote the manuscript.

COMPETING FINANCIAL INTERESTS
The authors declare no competing financial interests.

Europe PMC Funders Author Manuscripts

Compared to the regulation of microtubule growth, the molecular mechanisms underlying microtubule nucleation are poorly understood. In spindles centrosome-, chromatin-, kinetochore-, and microtubule-dependent nucleation pathways work in parallel controlling microtubule nucleation[1]. The chromatin-dependent pathway drives local stimulation of nucleation around chromosomes[8]. A central player is the small GTPase Ran, which in its GTP-bound form (Ran^{GTP}) dissociates spindle assembly factors (SAFs) from their inhibitory interaction with nuclear transport receptors importins[1]. Ran^{GTP} is produced locally around chromosomes[9-12]. The resulting Ran^{GTP} concentration gradient generates a gradient of SAFs released from importins triggering microtubule nucleation and spindle assembly in meiosis and mitosis[13-15]. The microtubule-dependent (branching) nucleation pathway, mediated by the augmin complex[16], is also controlled by Ran^{GTP} [17].

A major Ran pathway target required for chromatin-stimulated and augmin-mediated microtubule nucleation and spindle assembly is TPX2 (Targeting Protein for Xklp2)[17-19]. Depletion of TPX2 from XEE abolishes chromatin- and microtubule-dependent microtubule formation[17, 19]. Its expression in cells is tightly regulated[20]. Reduction of TPX2 levels increases aneuploidy and elevates frequency of spontaneous tumour development in mice[21], overexpression causes defects in microtubule organisation[20] and correlates with poor cancer prognosis and high metastasis frequency in humans[22].

TPX2 is a multifunctional protein. Its central domain mediates interactions with importin α[23, 24] explaining its Ran-dependence[19]. One or more potential microtubule binding sites reside either in the N-terminus or the central part of TPX2, possibly overlapping with the importin binding site[25, 26]. TPX2 interacts with several other proteins involved in spindle assembly[17, 18, 27-32].

The N-terminus of TPX2 activates and stabilises Aurora A kinase (AurA)[33-35]. Whether TPX2 acts exclusively via AurA on microtubule nucleation is unclear with contradicting results having been reported[17, 21, 26, 36-39]. Another important factor for Ran-dependent microtubule nucleation is the γ-tubulin ring complex (γ-TuRC)[40], which is thought to facilitate nucleation by templating initial microtubule assembly[40]. TPX2-dependent AurA activation can stimulate γ-TuRC activity in XEE[39]. However, the lack of TPX2 or γ-TuRC in chromatin-driven microtubule formation can be partially compensated independently of AurA, most efficiently by the excess of XMAP215[37]. This suggests that parallel pathways may exist, where multiple factors act on nucleation with distinct, yet partly overlapping activities. TPX2 enhances branching microtubule nucleation independently of its AurA interaction, but depending on its microtubule binding ability[17] pointing to a direct role of TPX2 in nucleation.

Early in vitro work reported that high concentrations of purified TPX2 induced the formation of tubulin aggregates and interconnected microtubule bundles[23, 26]. Yet, it remains unknown if at physiological levels purified TPX2 is sufficient to nucleate microtubules efficiently, or if additional factors are required. Kinetic measurements of how TPX2 affects microtubule dynamics and nucleation alone or in combination with other proteins implicated in localised microtubule formation are lacking. Therefore, the molecular mechanisms underlying the functionality of the protein network controlling chromatin-dependent

microtubule nucleation, and particularly the role of TPX2 herein, its interplay with XMAP215/chTOG and its regulation, are poorly understood.

Here we studied the direct effects of human TPX2 and chTOG on microtubule nucleation and dynamics using real-time fluorescence microscopy-monitored in vitro reconstitutions. We find that TPX2 interacts preferentially with growing microtubule ends at binding sites that are distinct from other autonomous microtubule end trackers. TPX2 prevents microtubule catastrophes and slows down shrinkage thereby increasing microtubule lifetimes. At physiological concentrations TPX2 strongly promotes microtubule nucleation by stabilising microtubule nucleation intermediates. Fast and efficient microtubule formation requires the additional microtubule polymerase activity of chTOG, which on its own displays only moderate microtubule nucleating activity. Importins inhibit combined TPX2:chTOG-mediated nucleation by blocking TPX2's ability to interact with nucleation intermediates. Together, our in vitro reconstitutions define the molecular mechanism underlying the functional synergy of a minimal TPX2:chTOG microtubule nucleation module and its regulation by importins.

RESULTS

chTOG is a microtubule polymerase

We produced human chTOG (Fig. 1a-b) and characterised the biochemical activity of this member of the XMAP215 protein family. Using a Total Internal Reflection Microscopy (TIRFM)-based in vitro assay (Fig. 1c) we investigated how chTOG fused to monomeric GFP (chTOG-mGFP) localised to dynamic microtubules and how it affected their growth. Microtubules were grown from immobilised microtubule "seeds", which were stabilised by the non-hydrolysable GTP analogue GMPCPP, and elongated in the presence of Atto647N-labelled tubulin and GTP[41]. Kymographs of dynamic microtubules showed that chTOG-mGFP accumulated at both growing and shrinking microtubule plus ends (Fig. 1d, Supplementary Video 1). chTOG also strongly accelerated microtubule growth, like other XMAP215 family members[3, 42-44] in a dose-dependent manner saturating at ~ 200 nM chTOG with a 17-fold faster growth velocity (Fig. 1e). Similarly to XMAP215[3], chTOG facilitated the depolymerisation of GMPCPP-stabilised microtubules in the absence of free tubulin (Fig. 1f). This in vitro characterisation of human chTOG establishes it as a bona fide microtubule polymerase.

TPX2 binds to dynamic microtubules with a preference for growing ends

We purified full-length and truncated versions of mGFP-tagged human TPX2 (Fig. 2a-b), which appeared to be monomeric under our experimental conditions (Supplementary Table 1). TIRFM showed full-length TPX2 accumulating all along growing microtubules, as expected[23]. This accumulation was already evident at low nanomolar concentrations (Fig. 2c, e). At sub-nanomolar concentrations, TPX2 bound preferentially to growing microtubule ends and to the GMPCPP-stabilised microtubule part (Fig. 2d, f, Supplementary Video 2). The GMPCPP lattice appears to induce a high affinity conformation of TPX2's binding site that is normally present at growing microtubule ends.

A truncated construct (mGFP-TPX2$^{\Delta N}$) lacking the N-terminal region which contains the AurA interaction site (Fig. 2a-b), bound more weakly to microtubules, but with same preferences as full-length TPX2 (Fig. 2g). An even shorter construct (mGFP-TPX2^{mini}) additionally lacking the C-terminus (Fig. 2a-b), retained identical binding preferences, but bound even more weakly (Fig. 2h). Therefore, the central part of the molecule is sufficient for TPX2's microtubule binding specificity, whereas the peripheral parts contribute to increasing binding affinity consistent with earlier reports of multiple microtubule binding regions in the protein[25, 26]. Neither full-length mGFP-TPX2 nor mGFP-TPX2^{mini} tracked shrinking microtubule ends (Fig. 2i-j).

TPX2 increases the lifetime of microtubules

TIRFM revealed that TPX2 had almost no effect on the growth speed of dynamic microtubules at concentrations ranging from microtubule end tracking conditions to complete lattice decoration (Fig. 3a). Nevertheless the microtubule lifetimes doubled in the presence TPX2 (Fig. 3b, g). This was mostly a consequence of a reduced catastrophe frequency (growth-to-shrinkage transitions) (Fig. 3c, Supplementary Fig. 1) and depolymerisation speed (Fig. 3f) under conditions when TPX2 bound all along the microtubule lattice. This slow-down of depolymerisation increases the depolymerisation time (Fig. 3i) augmenting the likelihood of rescues (shrinkage-to-growth transitions) during shrinkage (Fig. 3b), and reducing depolymerisation episode lengths (Fig. 3h). mGFP-TPX2^{mini} also inhibited catastrophes resulting in increased microtubule lifetimes, however at higher concentrations (Fig. 3c, g); it had no major effect on other dynamic instability parameters (Fig. 3d-f, h-i). In summary, full-length TPX2 increases microtubule lifetimes by acting as an anti-catastrophe factor and by slowing down depolymerisation, in agreement with a recent report[45].

TPX2 recognises a unique binding site at growing microtubule ends

We analysed the preferential binding of TPX2 to microtubule ends, using mostly TPX2^{mini}, which constitutes the functional core of TPX2 with respect to its microtubule interaction. Averaged mGFP-TPX2^{mini} intensity profiles demonstrated that TPX2 accumulated in a short region at growing microtubule ends (Fig. 4a). The length of this region increased with increasing growth speed, up to ~ 1 μm for the fastest tested condition (highest tubulin concentration) (Fig. 4a), somewhat reminiscent of the binding region of the established microtubule end binding protein EB1[46-48]. However, different from EB1 and other autonomous end binders, the length of the TPX2 binding region extended with the overall time the microtubule spent growing (Fig. 4b) and with increasing mGFP-TPX2^{mini} concentrations (Fig. 4c).

Single molecule experiments either in the absence or presence of an excess of Alexa647-labelled SNAP-TPX2^{mini} ('spike' experiment, Fig. 4d, left and right, Supplementary Figs. 2b, 3a) revealed that the TPX2 binding/unbinding turnover at the growing microtubule end was fast with a mean dwell time of 0.27 ms (= $1/k_{off}$ with k_{off} = 3.7 s^{-1}, Supplementary Fig. 3b). This suggests that the increase of the average length of the TPX2^{mini} accumulation region with increasing growth speed and time, or TPX2^{mini} concentration directly reflects an increase of the length of the underlying TPX2 binding region and a structural property of the

growing microtubule end. Single molecule turnover measured at increasing distances from the microtubule end (covering the TPX2^{mini} accumulation region) also reflected the microtubule conformation change away from the growing end (increasing dissociation constant k_{off} and decreasing association rate r_{on}, depending on the TPX2^{mini} concentration (Fig. 4e) and the duration of microtubule growth (Supplementary Fig. 3c)).

Single molecule turnover of mGFP-TPX2^{mini} on GMPCPP microtubules, to which TPX2 binds with high preference, was similarly fast as on growing microtubule ends (Supplementary Fig. 3d-e). Full-length TPX2 turned over more slowly agreeing with its higher binding strength (Supplementary Fig. 3f), yet dynamically, indicating absence of oligomerisation or aggregation, in contrast to previous observations[23, 39]. At microtubule ends growing in the presence of GTP the mGFP-TPX2^{mini} intensity fluctuated strongly (Fig. 4f). This may be a consequence of dynamic changes of the end structure of the unfinished tube as microtubules grow[49]. Interestingly, TPX2 also tended to accumulate on bent microtubules (Fig. 4g). Moreover, unlike EB1[50], TPX2 did not bind strongly along microtubules grown in the presence of another GTP analogue, GTPγS (Fig. 4h). Nevertheless, TPX2 still accumulated at the growing ends of GTPγS microtubules (Fig. 4h), further suggesting that it recognises a unique structural feature not strictly coupled to the nucleotide state at the distal end of the growing microtubule.

These data demonstrate that the TPX2 binding region at growing microtubule ends has distinct properties compared to other autonomous end tracking proteins.

Surface-immobilised chTOG mildly stimulates microtubule nucleation

To test if these autonomous end binders, chTOG and TPX2, which have complementary effects on microtubule dynamics, promote microtubule nucleation we developed a TIRFM-based assay for the real-time observation of microtubule formation. We produced biotinylated full-length chTOG and TPX2 and, for controls, a biotinylated monomeric kinesin rigor mutant (Kin1^{rigor}) (Supplementary Fig. 2a). The proteins were attached in an oriented manner via neutravidin to functionalised and polyethylene glycol (PEG)-passivated glass slides[41] (Fig. 5a, Supplementary Fig. 4a-b). After addition of fluorescently labelled tubulin and GTP to surface-immobilised chTOG, a few microtubule nucleation and growth events were observed (Fig. 5b, second and third row, Supplementary Video 3), similar to previous observations with XMAP215[51]. This effect was specific, because no microtubules were observed on a Kin1^{rigor} control surface (Fig. 5b, top row, Supplementary Video 3), and it proportionally increased with chTOG concentration (Fig. 5c, left, Supplementary Fig. 4c).

Surface-immobilised TPX2 stabilises and arrests nucleation intermediates

When biotinylated TPX2 was surface-immobilised, a granular mass of tubulin (‘stubs’) was recruited to the surface (Fig. 5b, bottom two rows, Supplementary Video 3), very different from the observations with immobilised chTOG. Only few microtubules were observed after more than 10 min. Accumulation of stubs occurred over several minutes (Fig. 5c, right) in a dose-dependent manner increasing with higher TPX2 densities (Fig. 5b-c, right, Supplementary Fig. 4b-c) and increasing tubulin concentrations (Supplementary Fig. 4d-e). Since TPX2 does not interact strongly with soluble tubulin dimers (Supplementary Fig. 4f),

it may specifically stabilise larger tubulin assemblies on the surface that could represent nucleation intermediates[52-54]. However, these structures failed to transform into elongating microtubules, raising the question if additional activities could overcome the apparent arrest of microtubule formation.

The combined action of immobilised TPX2 and soluble chTOG promotes efficient microtubule nucleation

Remarkably, addition of chTOG to the assay with surface-immobilised TPX2 caused strong microtubule nucleation and growth within minutes (Fig. 5d, second and third row, Supplementary Video 4), in marked contrast to the absence of chTOG (Fig. 5d, first row). When immobilised TPX2 was replaced by biotinylated $Kin1^{rigor}$, only few microtubules formed in the presence of soluble chTOG (Fig. 5d, fourth and fifth row, Supplementary Video 4), similar to the effect of immobilised chTOG alone (Fig. 5b, second and third row), emphasizing the specificity of TPX2 activity in combination with chTOG. Microtubule end binding protein EB1 could not functionally substitute for chTOG in the nucleation assay with surface-immobilised TPX2, potentially due to lack of a growth promoting effect under these conditions, and mostly only stubs were observed (Supplementary Fig. 5).

These results demonstrate that the combined action of immobilised TPX2 and chTOG synergistically stimulate efficient microtubule nucleation and growth. It appears that on the TPX2-coated surfaces, chTOG can overcome a hindered transformation of nucleation intermediates into microtubules.

In solution TPX2 nucleates microtubules more efficiently than chTOG

To test whether immobilisation of TPX2 prevents the transformation of TPX2-induced nucleation intermediates, we modified the nucleation assay (Fig. 6a). We pre-incubated biotinylated TPX2 together with tubulin and GTP in solution before transferring the reaction mixture onto a functionalised neutravidin-coated glass surface, followed by TIRFM imaging. Strikingly within minutes, biotinylated TPX2 induced massive nucleation of slowly growing microtubules (Fig. 6b, middle row, Supplementary Video 5). Hence in solution, TPX2-induced nuclei can transform into microtubules, a conformational change that is apparently inhibited when nuclei form directly on a TPX2 surface (Fig. 5b, bottom two rows). In contrast to TPX2, biotinylated chTOG promoted the nucleation of only few, fast growing microtubules in this ‘solution’ nucleation assay (Fig. 6b, top row, Supplementary Video 5), similar to observations in the ‘surface’ assay (Fig. 5b, second and third row). Nucleation promoting activities of both proteins were dose-dependent (Fig. 6c-d), with TPX2 promoting the appearance of an increasingly denser mass of shorter microtubules as opposed to fewer longer microtubules by chTOG (Fig. 6c). Hence in solution, TPX2 is considerably more efficient in promoting microtubule nucleation than chTOG, although TPX2 hardly accelerates microtubule growth.

Similar to the ‘surface’ nucleation assay (Fig. 5d), the efficiency of microtubule nucleation was enhanced by the combined action of TPX2 and chTOG (Fig. 6b, bottom row, Supplementary Video 5). Again, EB1 did not stimulate TPX2’s nucleating activity or have

an effect on chTOG-mediated microtubule nucleation (Supplementary Fig. 6). This further demonstrates the specificity of chTOG:TPX2 microtubule nucleation module.

The central part of TPX2 is sufficient to stimulate microtubule nucleation

TPX2^{mini} also stimulated microtubule nucleation in solution in a dose-dependent manner (Fig. 7a, top two rows), however requiring higher concentrations than full-length TPX2, agreeing with its weaker microtubule binding (Fig. 2). Combining TPX2^{mini} and chTOG again further amplified microtubule formation (Fig. 7a, bottom row). Moreover, similarly to full-length TPX2, the minimal construct as well as TPX2$^{\Delta N}$ also appear to promote microtubule nucleation via stabilisation of microtubule nucleation intermediates as suggested by the recruitment of 'stubs' when only surface-immobilised protein is present in the assay (Fig. 7b, Supplementary Fig. 7, Supplementary Video 6). Therefore, the central part of TPX2 that contains its core microtubule binding domain and the importin interaction region also harbours its basic microtubule nucleating activity.

Importin α/β regulates synergistic TPX2/chTOG-dependent microtubule nucleation by interfering with TPX2's binding to nucleation intermediates

In XEEs, TPX2's nucleating activity is inhibited by importin α/β[19, 23, 26]. The mechanism of how this interaction inhibits TPX2 is still debated. Therefore, we produced human importin α and β (Supplementary Fig. 2d) and investigated whether importins are sufficient to regulate the efficiency of TPX2:chTOG-dependent microtubule nucleation.

In our nucleation assay with immobilised Kin1^{rigor} on the surface, the addition of importins to chTOG had no effect on the mild nucleation promoting effect of chTOG (Fig. 8a, first and second row, Supplementary Video 7). The combination of full-length mGFP-TPX2 and chTOG caused dramatic microtubule nucleation and growth (Fig. 8a, third row, Supplementary Video 7), as in the previous experiments (Fig. 5d, Fig. 6b). mGFP-TPX2 decorated the nucleated microtubules (Fig. 8a, third row), as expected for this TPX2 concentration (Fig. 2c). Addition of excess importin α/β to TPX2 and chTOG strongly suppressed nucleation (Fig. 8a, fourth row) down to levels observed with chTOG alone (Fig. 8a, first and second rows), demonstrating that importins indeed inhibit synergistic TPX2:chTOG-dependent microtubule nucleation. TPX2 association with the few nucleated microtubules was severely reduced (Fig. 8a, bottom row). Importins also blocked TPX2's interaction with nucleation intermediates as their recruitment by surface-immobilised TPX2 was severely suppressed by importins (Fig. 8b). Thus, the inhibition of TPX2:chTOG-mediated microtubule nucleation by importins is a consequence of interfering with TPX2's stabilisation of nucleation intermediates.

DISCUSSION

How microtubule nucleation is controlled during cell division is a major open question. Multiple proteins whose interrelations are currently poorly understood are required for the Ran-dependent chromatin-[37] and augmin-stimulated nucleation pathways[17] in spindle assembly. Our TIRFM-based in vitro reconstitutions show that the Ran pathway target TPX2

and the Ran-independent chTOG are two key players that cooperate in efficient microtubule nucleation.

We showed here that chTOG supported microtubule formation in solution rather weakly, presumably by its growth promoting activity. TPX2 however strongly stimulated nucleation likely by directly stabilising early nucleation intermediates. Differences to previous in vitro work[23, 26] may well be explained by different assay conditions. Here under real-time imaging conditions (no fixatives), physiological concentrations of TPX2 (100 nM in XEE[19]) strongly stimulated nucleation albeit with slow microtubule growth. During spindle assembly efficient nucleation is combined with fast growth to achieve the rapid production and maintenance of a large dynamic microtubule mass[1, 37]. The minimal TPX2:chTOG microtubule nucleation module harbours these critical activities. Importins control this module by inhibiting TPX2-mediated stabilisation of nucleation intermediates, providing a potential mechanism for Ran-dependent localisation of microtubule nucleation in vivo.

Microtubule ‘nuclei’ may be viewed as growing microtubule end regions preceding the closed tube (Fig. 8c). Therefore, understanding how TPX2 and chTOG localise to and act on growing microtubule ends can provide insight into the molecular mechanism of how these two proteins facilitate microtubule nucleation. In contrast to short-lived nucleation intermediates[52] growing ends can be readily observed at steady state. Whereas chTOG showed the conserved behaviour of a microtubule polymerase, TPX2 suppressed microtubule catastrophes and reduced the depolymerisation speed, strongly stabilising dynamic microtubules without having a strong effect on the growth speed. Hence, these proteins affect different microtubule dynamic instability parameters, acting in a complementary manner.

Autonomous microtubule end binding as observed for chTOG is well established for this protein family[3, 42, 44, 55], however it has not been described for TPX2 before. TPX2 behaved very differently from other end binders with characteristics that help to explain its role in microtubule nucleation. First, TPX2 stabilises its own binding sites at growing microtubule end regions by slowing down their transformation into mature lattice sites. This is likely at the origin of its stabilising effects on dynamic microtubules and nucleation intermediates. Second, TPX2 has a remarkably high preference for binding to GMPCPP microtubules. GMPCPP is considered the most GTP-like nucleotide analogue, and it strongly promotes microtubule nucleation and stabilisation[56]. The longitudinal inter-tubulin spacing in GMPCPP microtubules is longer than that of GDP microtubules[57, 58]. This spacing or another feature of a high affinity conformation of the yet unknown TPX2 binding site displayed by the GMPCPP lattice may possibly reflect a structure present at growing microtubule ends and nucleation intermediates with a favourable curvature, potentially different from that of the fully closed tube. This view is supported by TPX2’s stronger binding to bent microtubules. Such curvature sensing was proposed for the neuronal microtubule-stabilising protein doublecortin[59] and XMAP215 family microtubule polymerases[60].

In summary, TPX2 recognises a conformation that is absent in mature microtubules and may well be related to the curved tapered or sheet-like extensions observed at growing ends[49, 61]

and to the still poorly understood structure of microtubule 'nuclei'[52-54]. Interestingly, immobilised TPX2 can arrest the transformation of stabilised nucleation intermediates into microtubules, suggesting that a large-scale conformational change such as tube closure is required. This closure can be promoted by the growth promoting activity of chTOG, suggesting that longer protofilaments with extended lateral contacts could facilitate the curvature change from nucleation intermediate to a microtubule[49].

Our in vitro reconstitution of a synergistic nucleation module consisting of TPX2 and chTOG can explain why in XEE, both TPX2 and XMAP215 are required for Ran^{GTP}-dependent microtubule formation around chromatin[4, 19, 37] and why TPX2 facilitates microtubule nucleation from XMAP215 beads in this experimental system[62]. Ran^{GTP}-driven microtubule nucleation in cells and in XEE also requires the master nucleator γ-TuRC[37], which provides a structural template for assembling the helical microtubule lattice[40]. Posttranslational modifications or interactions with binding/targeting partners inducing conformational changes in γ-TuRC have been proposed to modulate its activity[40]. To integrate previous observations in a model, conceptually, the process of microtubule nucleation in cells may be divided into three phases: (1) Initial templated assembly of tubulins onto the γ-TuRC surface; (2) growth of a nucleation intermediate consisting of many tubulins that might resemble the tapered or sheet-like structure of growing microtubule ends; (3) closure of this intermediate assembly into a tube with typical GDP lattice characteristics.

This scenario would allow for multiple opportunities to regulate the nucleation efficiency. First, at the level of the γ-TuRC-mediated templating activity, for example by one of TPX2's indirect effects - phosphorylation of γ-TuRC interaction partners by TPX2-activated AurA[39]. Second, at the level of the nucleation intermediate that extends from the γ-TuRC template by the direct stabilisation of the unfinished lattice by TPX2 together with acceleration of its elongation by chTOG (Fig. 8c). Interestingly, both of these proteins were recently also reported to facilitate the initiation of growth from stable microtubule nucleation templates in vitro[45]. Finally, microtubule nucleation efficiency could be controlled at the level of protofilament growth and initial tube closure. Different types of regulatory input from overlapping pathways could easily be integrated in such a model: global regulation by constitutively active players such as chTOG, local regulation from the Ran pathway via TPX2's direct and indirect activities, and temporal control from cell cycle-dependent posttranslational modifications.

In the future, the extension of the in vitro reconstitution of the minimal nucleation module studied here by including additional regulatory factors, will allow the systematic dissection of the individual contributions of different proteins. Together, this will lead to a systems level understanding of the complex regulatory microtubule nucleation network and spindle assembly.

METHODS

Cloning and protein biochemistry

Human TPX2—The full-length protein coding sequence of human TPX2 (1-747 aa) was amplified by PCR using its cDNA as template (NM_012112.4, Origene) and cloned into modified pFastBacHta-based vectors. In these vectors the His_6 tag had been replaced with a StrepTagII (WSHPQFEK) (pFastBacSTREP), and either a monomeric green fluorescent protein (mGFP)[63, 64], or a SNAP-tag coding sequence (NEB) had been inserted after the TEV protease cleavage site present in the original vector. This enabled the construction of expression plasmids for N-terminal fusion proteins of TPX2: StrepTagII-mGFP-G_5A-TPX2 and StrepTagII-SNAP-G_5A-TPX2 in which StrepTagII could be cleaved off by TEV protease treatment (Supplementary Table 2), final protein products being referred to as mGFP-TPX2 and SNAP-TPX2 throughout the manuscript. Expression vectors for similar N-terminal fusions of truncated versions of human TPX2 ($TPX2^{\Delta N}$: 274-747 aa; $TPX2^{mini}$: 274-659 aa) were constructed in the same manner, referred to as mGFP-$TPX2^{\Delta N}$, mGFP-$TPX2^{mini}$, and SNAP-$TPX2^{mini}$. In order to generate TPX2, $TPX2^{\Delta N}$, and $TPX2^{mini}$ expression constructs that could be biotinylated, the respective coding regions were cloned into a modified pFastBacDual vector under the control of a polyhedrin promoter to form an N-terminal fusion with Biotin Acceptor Peptide (BAP: GLNDIFEAQKIEWHE) followed by a G_5-linker, monomeric blue fluorescent protein coding sequence (mTagBFP, Evrogen), and another G_5A linker resulting in BAP-G_5-mTagBFP-G_5A-TPX2 (or $TPX2^{\Delta N}$, or $TPX2^{mini}$, respectively) (Supplementary Table 2), referred to as biotinylated TPX2, biotinylated $TPX2^{\Delta N}$, or biotinylated $TPX2^{mini}$. The P10 promoter in the same pFastBacDual vector drives the expression of *Escherichia coli* biotin ligase BirA to facilitate biotinylation of the acceptor tag during protein expression in insect cells. Baculovirus preparation and protein expression in baculovirus-infected insect cells (*Sf*21) for TPX2 constructs (but also all the other baculovirus-expressed proteins) were carried out using Bac-to-Bac system (Life Technologies) following the manufacturer's instructions.

Sf21 cells expressing StrepTagII-containing TPX2 proteins were resuspended in ice-cold lysis buffer (50 mM HEPES, 300 mM KCl, 25 mM sucrose, 1 mM EDTA, 5 mM 2-mercaptoethanol (2-ME), pH 8.0) supplemented with 5 mM $MgCl_2$, protease inhibitors (complete EDTA-free protease inhibitor mix, Roche), DNAse I (10 μg/ml, Sigma-Aldrich), and 10 mg of avidin per 1 litre of insect cell culture to absorb biotin from the cell culture medium (that would otherwise inhibit protein binding to affinity matrix by competition). Resuspended cells were lysed by douncing (40 strokes), the lysate was then clarified by ultracentrifugation (183,960 × *g*, 45 min, 4°C) and loaded on a StrepTrap HP column (GE Healthcare). After washing the column with lysis buffer, proteins were eluted with lysis buffer supplemented with 2 mM $MgCl_2$, protease inhibitors, 50 mM arginine, 50 mM glutamate, and 2.5 mM D-desthiobiotin. The N-terminal StrepTagII was cleaved off by overnight incubation with Tobacco Etch Virus (TEV) protease on ice. In case of SNAP-tagged proteins, SNAP-Surface® Alexa Fluor® 647 (NEB) was added in the same reaction to label the protein fluorescently. The buffer was then changed to MES A buffer (20 mM MES, 2 mM $MgCl_2$, 5 mM 2-ME, pH 6.0) via HiPrep 26/10 Desalting columns (GE Healthcare). Next, the protein was again run over the StrepTrap HP column to remove any

uncleaved products that still contained the StrepTagII. The flow-through was pooled and loaded on a MonoS 5/50 GL column (GE Healthcare) pre-equilibrated with MES A buffer. The column was then washed with the same buffer and the protein was subsequently eluted using an increasing KCl concentration gradient in MES A buffer. Peak fractions were pooled and subjected to size exclusion chromatography using Superose 6 10/300 GL column (GE Healthcare) in TPX2 storage buffer (50 mM HEPES, 300 mM KCl, 2 mM $MgCl_2$, 250 mM sucrose, 50 mM arginine, 50 mM glutamate, 5 mM 2-ME, pH 7.5). The peak fractions were pooled, concentrated via Vivaspin 15R concentrators (30,000 MWCO, Sartorius), ultracentrifuged (278,088.3 × *g*, 10 min, 4°C), aliquoted, snap frozen, and stored in liquid nitrogen. In case of mGFP-TPX2$^{\Delta N}$, the ion exchange step was bypassed and, instead, after TEV cleavage, the buffer was immediately exchanged to TPX2 storage buffer, the protein was then run over a StrepTrap HP column, concentrated via Vivaspin concentrators, ultracentrifuged, and subjected to size exclusion chromatography, and processed as described above.

For the purification of *in vivo* biotinylated TPX2 proteins, the clarified was buffer-exchanged via HiPrep 26/60 Desalting columns to fresh lysis buffer to remove biotin present in the insect cell growth medium. The lysate was then incubated with immobilized monomeric avidin resin (Thermo Scientific). After washing the resin with lysis buffer, proteins were eluted with lysis buffer supplemented with 2 mM $MgCl_2$, protease inhibitors, 50 mM arginine, 50 mM glutamate, and 2 mM biotin. The buffer was then exchanged to TPX2 storage buffer and the purification concluded with size-exclusion chromatography (Superose 6 10/300 GL) as described above for the mGFP-TPX2$^{\Delta N}$.

Human chTOG—The full-length protein coding sequence of human chTOG (1-2032 aa, NP_001008938.1) was amplified by PCR using a plasmid containg its cDNA as a template (generously provided by Stephen Royle) and cloned into the pFastBacSTREP vector described above resulting in StrepTagII-chTOG in which StrepTagII could be cleaved off by TEV protease treatment (Supplementary Table S2), creating a final protein product chTOG as referred to in this manuscript. To generate an mGFP-tagged version of chTOG, an mGFP coding sequence was inserted to the C-terminus of the chTOG coding region in the same construct to create StrepTagII-chTOG-A_2G_5-mGFP, where the StrepTagII could again be removed by TEV protease, creating a final product referred to as chTOG-mGFP. In order to generate a chTOG construct that could be biotinylated, its coding region was cloned into a modified pFastBacDual vector under the control of a polyhedrin promoter to form a C-terminal fusion with mTagBFP followed by a G_5-linker and BAP. The chTOG coding region was separated from the rest of the tag by a G_5-linker. The resulting construct chTOG-G_5-mTagBFP-G_5A-BAP (Supplementary Table 2) is referred to as biotinylated chTOG. The P10 promoter in the same pFastBacDual vector again drives the expression of biotin ligase BirA, *Sf21* cells expressing recombinant chTOG proteins were resuspended in ice-cold chTOG storage buffer (50 mM Na-phosphate, 400 mM KCl, 2 mM $MgCl_2$, 0.005% (vol/vol) Brij-35, 5 mM 2-ME, pH 7.2) supplemented with protease inhibitors, DNAse I (10 μg/ml, Sigma-Aldrich), and 10 mg of avidin. Resuspended cells were lysed by douncing (40 strokes), lysate was then clarified by ultracentrifugation (183,960 × *g*, 45 min, 4°C) and loaded on the StrepTrap HP column. After washing the column with chTOG storage buffer,

proteins were eluted with the same buffer supplemented with 2.5 mM D-desthiobiotin. The N-terminal StrepTagII was cleaved off by overnight incubation with TEV protease on ice. The buffer was then changed back to chTOG storage buffer buffer via HiPrep 26/10 Desalting columns to remove D-desthiobiotin. Next, the protein was again run over the StrepTrap HP column. The flow through was pooled, concentrated with Vivaspin 15R concentrators (30,000 MWCO), ultracentrifuged (278,088.3 × *g*, 10 min, 4°C), and separated by size-exclusion chromatography using Superose 6 10/300 GL column. The peak fractions were pooled, concentrated, and ultracentrifuged, aliquoted, snap frozen, and stored in liquid nitrogen.

For the purification of *in vivo* biotinylated chTOG protein, the clarified lysate was buffer-exchanged via HiPrep 26/60 Desalting columns to fresh lysis buffer to remove biotin. The lysate was then incubated with immobilized monomeric avidin resin (Thermo Scientific). Resin was washed with lysis buffer, followed by protein elution with lysis buffer supplemented with 2 mM biotin and protease inhibitors. The buffer was then exchanged back to chTOG lysis buffer via HiPrep 26/60 Desalting columns. Protein containing fractions were pooled and concentrated and the purification was concluded with size-exclusion chromatography (Superose 6 10/300 GL) in chTOG storage buffer as described above.

Human EB1—Untagged human EB1 protein was expressed and purified as described previously65, except that size-exclusion chromatography via Superdex 200 10/300 GL column (GE Healthcare) was carried out in EB1 storage buffer: 25 mM K-phosphate, 350 mM NaCl, 2 mM MgCl2, 5 mM 2-ME, pH 7.4.

Monomeric Drosophila kinesin 1 rigor mutant—In order to generate a construct that could be biotinylated, the coding sequence of the monomeric *Drosophila melanogaster* kinesin 1 rigor mutant (1-340 aa, T99N) was amplified by PCR using pEY4-Kin401-T99N as template and cloned into modified pRSFDuet1 plasmid to create an N-terminal fusion protein: BAP-G_5-mTagBFP-EFG_5-Kin^{rigor}, referred to as biotinylated $Kin1^{rigor}$ The second T7 promoter of this vector drives the expression of the BirA biotin ligase (Supplementary Table 2).

The fusion protein was expressed in *Escherichia coli* BL21 pRIL strain at 18°C for 16 hours induced by 0.1 mM IPTG in the presence of 7 μg/ml biotin to facilitate biotinylation of the protein. In order to purify biotinylated Kin^{rigor} protein, the cells were resuspended in lysis buffer (50 mM Na-phosphate, 350 mM KCl, 5 mM $MgCl_2$, 0.2 mM ATP, 1 mM EDTA, 1 mM 2-ME, pH 7.2) supplemented with protease inhibitors and DNAse I and lysed using a microfluidiser. The lysate was clarified by ultracentrifugation (183,960 × *g*, 45 min, 4°C), the clarified lysate was then filtered through a 0.22 μm bottle-top filter (Millipore) followed by buffer exchange via HiPrep 26/60 Desalting columns to fresh lysis buffer to remove biotin. The lysate was then incubated with immobilized monomeric avidin resin. After washing the resin with lysis buffer, proteins were eluted with lysis buffer supplemented with 2 mM biotin. The buffer was then exchanged to $Kin1^{rigor}$ storage buffer (50 mM Na-phosphate, 350 mM KCl, 1 mM $MgCl_2$, 0.1 mM ATP, 1 mM 2-ME) via HiPrep 26/60 Desalting columns, and supplemented with fresh protease inhibitors. The sample was

subsequently concentrated using Vivaspin 15R concentrators, followed by ultracentrifugation (278,088.3 × *g*, 10 min, 4°C) and separation by size-exclusion chromatography using a Superdex 200 16/60 column (GE Healthcare). The peak fractions were pooled, concentrated and ultracentrifuged, supplemented with 20 % glycerol (vol/vol; final concentration), aliquoted, snap frozen, and stored in liquid nitrogen.

Human importin α and β—Full-length protein coding sequences of human importin α and β were amplified by PCR using their cDNA containing plasmids as templates (kindly provided by Rebecca Heald) and cloned into pETMZ vector to generate expression constructs: His_6-Ztag-Impα and His_6-Ztag-Impβ where the His_6-Ztag could be removed by TEV protease treatment (Supplementary Table 2).

Importin α and β fusion proteins were expressed and purified in a similar manner to each other. Protein expression was induced in *Escherichia coli* BL21 pRIL by 0.1 mM IPTG at 18°C for 16 hours. In order to purify either of these proteins, cells were resuspended in lysis buffer (50 mM HEPES, 400 mM KCl, 10 mM $MgCl_2$, 2.5 mM EDTA, 25 mM sucrose, 2 mM imidazole, 5 mM 2-ME, pH 7.2) supplemented with protease inhibitors and DNAse I and lysed using a microfluidiser. The lysate was clarified by ultracentrifugation (183,960 × *g*, 45 min, 4°C) and then incubated with Protino Ni-TED resin (Macherey-Nagel). After washing the resin with lysis buffer, proteins were eluted with elution buffer (50 mM HEPES, 300 mM KCl, 2 mM $MgCl_2$, 2.5 mM EDTA, 25 mM sucrose, 400 mM imidazole, 5 mM 2-ME, pH 8.0). The protein containing fractions were pooled and the buffer was immediately exchanged to importin storage buffer (50 mM HEPES, 300 mM KCl, 2 mM $MgCl_2$, 250 mM sucrose, 5 mM 2-ME) via PD-10 Desalting columns (GE Healthcare). The N-terminal His_6-Ztag was cleaved off by overnight incubation with TEV protease on ice. The sample was subsequently concentrated using Vivaspin 15R concentrators, followed by ultracentrifugation (278,088.3 × *g*, 10 min, 4°C) and separation by size-exclusion chromatography using a Superdex 200 16/60 column (GE Healthcare). The peak fractions were pooled, concentrated, ultracentrifuged, aliquoted, snap frozen, and stored in liquid nitrogen.

Tubulin—Porcine brain tubulin was purified as described[66] and for fluorescence microscopy assays labelled with Atto565-N-hydroxysuccinimide ester (NHS; Sigma-Aldrich), or Atto647N-NHS ester (Sigma-Aldrich), or biotin-NHS ester (Thermo Scientific) according to published methods[67].

The sequences of all newly cloned constructs were verified by sequencing. All protein purifications were carried out at 4°C. Protein concentrations were determined either using a Bradford protein assay, or for tubulin, by measuring the absorbance at 280 nm. Protein concentrations refer to monomers, except for tubulin concentrations, which refer to dimers.

Size-Exclusion Chromatography Multi-Angle Light Scattering Analyis (SEC-MALS) of TPX2 constructs

TPX2, $TPX2^{\Delta N}$, $TPX2^{mini}$ and bovine serum albumin (Sigma-Aldrich) were buffer exchanged into SEC-MALS buffer containing 50 mM HEPES (pH 7.5), 150 mM KCl, 2 mM $MgCl_2$, 50 mM arginine, 50 mM glutamate, 0.005% (vol/vol) Brij-35, 5 mM 2-ME and

ultracentrifuged (278,088.3 × *g*, 10 min, 4°C). The samples (40 µl volume, at 2 – 3 µg/µl concentration) were then subjected to size exclusion chromatography using Superose 6 3.2 300 (GE Healthcare) in conjunction with MALS (DAWN8+/OptiLab t-REX; Wyatt) at room temperature. Three independent runs were performed for each construct.

Size-exclusion chromatography to test tubulin:TPX2 interaction

Tubulin and TPX2 were buffer exchanged to an ice cold buffer containing 80 mM PIPES (pH 6.8), 60 mM KCl, 1 mM $MgCl_2$, 1 mM EGTA, 0.005% (vol/vol) Brij-35, 5 mM 2-ME. The proteins were then ultracentrifuged (278,088.3 × *g*, 10 min, 4°C) and diluted in the same buffer either alone or in combination at indicated concentrations. These samples were incubated on ice for 15 min before loading (400 µl volume) on Superose 6 Increase column (GE Healthcare) at 4°C. Tubulin:TPX2 interaction experiment was performed once for each tubulin:TPX2 ratio.

Total Internal Reflection Fluorescence (TIRF) Microscopy

Flow chambers for assays were assembled from biotin-polyethylene glycol (PEG)-functionalized glass and poly (L-lysine)-PEG (SuSoS) passivated counter glass as described previously[41]. All experiments were imaged at 30°C ± 1°C on a TIRF microscope (iMIC, FEI Munich) described in detail previously[48, 65] unless indicated otherwise. Image acquisition and channel alignment were carried out as explained previously[48,65]. Exposure times were between 60 ms (single molecule assays) and 150 ms (nucleation assays). Images were acquired either after every 60 ms (single molecule imaging on dynamic microtubules), 100 ms (single molecule imaging on GMPCPP-stabilised microtubules), 250 ms (localisation studies, microtubule end tracking experiments) or 2 s (microtubule lifetime measurements, nucleation assays). Laser powers as well as exposure times and acquisition frame rate were kept constant within a set of experiments to allow for direct comparisons between different conditions.

Dynamic microtubule assays—GMPCPP-stabilised biotinylated fluorescently labelled microtubule “seeds” for assays with dynamic microtubules were prepared as described[43] (containing 12% of either Atto647N- or Atto565-labelled tubulin). The assay itself is a modification of the protocol developed earlier[41]. In short, a flow chamber was sequentially incubated for 5 min with 5% Pluronic F-127 in MQ water (Sigma-Aldrich) at room temperature, washed with assay buffer (AB: 80 mM PIPES, 60 mM KCl, 1 mM EGTA, 1 mM $MgCl_2$, 1 mM EGTA, 1 mM GTP, 5 mM 2-ME, 0.15% (w/vol) methylcellulose (4,000 cP; Sigma-Aldrich), 1% (w/vol) glucose, 0.02% (vol/vol) Brij-35) supplemented with 50 µg/ml κ-casein (Sigma-Aldrich), then incubated for 2 min on a metal block on ice in the same buffer additionally containing 50 µg/ml of NeutrAvidin (Life Technologies). The chamber was subsequently washed with AB and then incubated with AB containing an appropriate dilution of GMPCPP-stabilised microtubule “seeds” for 3 min at room temperature. Following additional washes with AB, a final assay mix (below) was flowed into the chamber and imaging was started 1 min after placing the chamber on microscope. Composition of the final assay mix: 75% (vol/vol) AB, oxygen scavengers (180 µg/ml catalase (Sigma-Aldrich), 750 µg/ml glucose oxidase (Serva)) diluted in BRB80 (80 mM PIPES, 1 mM EGTA, 1 mM $MgCl_2$), varying concentrations of tubulin (containing 5% of

either Atto647N- or Atto565-labelled tubulin) in BRB80, and different mGFP-TPX2 or Alexa647-labelled SNAP-TPX2, or chTOG and chTOG-mGFP constructs diluted in their storage buffers. In order to keep the buffer composition of the final assay mix unchanged within a set of experiments and to allow for direct comparisons between experiments, the overall BRB80 and storage buffer content was kept constant within one set of experiments.

Single molecule assay on GMPCPP microtubules—Samples were prepared as described above for the dynamic microtubule assays; however GTP and tubulin were omitted from the final assay mix.

GMPCPP microtubule depolymerisation assay—This assay was performed essentially as initially described elsewhere[3]. Samples were prepared as summarised for the dynamic microtubule assays, using the same buffers and sequence of incubation steps, however GTP and tubulin were omitted from the final assay mix.

'Surface' microtubule nucleation assay—A flow chamber was sequentially incubated for 5 min with 5% Pluronic F-127 in MQ water at room temperature, washed with AB (described above) supplemented with 50 μg/ml κ-casein, then incubated for 2 min on a metal block on ice in the same buffer additionally containing 50 μg/ml of NeutrAvidin. The chamber was subsequently washed with TPX2 storage buffer (described above) and then incubated with an indicated concentration of protein constructs (biotinylated $Kin1^{rigor}$, biotinylated chTOG, biotinylated TPX2, biotinylated $TPX2^{\Delta N}$, or biotinylated $TPX2^{mini}$) diluted either in TPX2 storage buffer (Fig.-s 5b-c, 8a-b, Supplementary Fig. 4a-e,), or in AB (Fig. 5d, Fig. 7b, Supplementary Fig. 7) for 10 min on a metal block on ice. Following washes with AB at room temperature, a final assay mix (below) was flowed into the chamber, which was then sealed with nail polish. Imaging was started 1 or 2 min after placing the chamber on the microscope. Composition of the final assay mix: 75% (vol/vol) AB, oxygen scavengers (180 μg/ml catalase, 750 μg/ml glucose oxidase) diluted in BRB80, 12.5 μM tubulin (containing 5% Atto647N-labelled tubulin) in BRB80, 1 mg/ml bovine serum albumin (Sigma-Aldrich) in BRB80, and the indicated concentrations of mGFP-TPX2, chTOG, or EB1 diluted in their own storage buffers, and importin α/β complex, which had been individually buffer exchanged to AB using Zeba™ Micro Spin Desalting Columns (7K MWCO, Thermo Scientific), and then premixed in AB. When the effect of importins on microtubule nucleation was tested in the presence of surface-immobilised TPX2 (Fig. 8b), additional 3 min incubation step with 500 nM importin α/β complex (buffer exchanged as described above) at room temperature was included before flowing in the final assay mix containing Atto64N-labeled tubulin in the absence or presence of 500 nM importin α/β. Similarly to the dynamic microtubule assays, the buffer composition of the final assay mix remained unchanged to allow for direct comparisons between different experiments within one set of experiments.

'Solution' microtubule nucleation assay—The 'solution' nucleation was based on the 'surface' nucleation assay with the following modifications. While the flow chamber was incubated with Pluronic F-127 for 10 min, the final assay mix, as in the 'solution' nucleation assay, but now also including the biotinylated protein (either chTOG or TPX2) at the

indicated concentration, was mixed on ice and ultracentrifuged (278,088.3 × *g*, 10 min, 4°C). In parallel, the flow chamber was washed with AB (described above) supplemented with 50 μg/ml κ-casein, and then incubated for 2 min on a metal block on ice with the same buffer that additionally contained 50 μg/ml of NeutrAvidin. The flow chamber was then washed with AB at room temperature and placed in a microscope heating box at 30°C. The ultracentrifuged final assay mix was transferred to 30°C to initiate nucleation in solution. After 1 min this nucleation mix was quickly flowed through the pre-warmed flow chamber. The chamber was sealed with nail polish. Imaging was started 1.5 min after placing the chamber on the microscope.

Data analysis and image processing are described in detail in the accompanying Supplementary Note.

Reproducibility

Experiments were repeated three times, unless indicated otherwise. Representative images are shown. Number of events (number of microtubule growth and depolymerisation episodes, rescues and catastrophes, total polymerisation and depolymerisation time) measured for calculating microtubule dynamic instability parameters for different conditions, as well as statistics information is included in the figure legends. In case data for quantifications from less than three datasets were used (Fig. 1e and 3a, Supplementary Fig. 1a, and 5b), the datasets themselves were large and the described effects were observed reproducibly (dose-dependent growth promoting effect of chTOG, lack of growth promotion by TPX2 or EB1 under these conditions, and the prevention of microtubule minus end catastrophes by TPX2). Corresponding information about TPX2 microtubule end binding analysis (presented on Fig. 4 and Supplementary Fig. 3) can be found in the additional Supplementary Note.

Supplementary Material

Refer to Web version on PubMed Central for supplementary material.

ACKNOWLEDGEMENTS

We thank Iris Lüke and Claire Thomas for insect cell culture maintenance; Claire Thomas for help with protein expression, and cloning and purification of the biotinylated Kin1^{rigor} construct; Christian Düllberg for a partially purified MonoQ fraction of the untagged human EB1 protein. We are grateful for Rebecca Heald, Dirk Görlich, Stephen Royle, Günter Stier, and Isabelle Vernos for kindly providing various plasmids. We thank all the members of the Surrey lab for discussions, and Franck Fourniol and Christian Düllberg for critical reading of the manuscript. T.S. acknowledges the ERC (Project 323042) and Cancer Research UK for funding, J.R. was supported by a Cancer Research UK postdoctoral fellowship, an EMBO Long-Term Fellowship (LTF-615-2012), and a Sir Henry Wellcome Postdoctoral Fellowship (100145/Z/12/Z).

REFERENCES

1. Helmke KJ, Heald R, Wilbur JD. Interplay between spindle architecture and function. Int Rev Cell Mol Biol. 2013; 306:83–125. [PubMed: 24016524]
2. Gard DL, Kirschner MW. A microtubule-associated protein from Xenopus eggs that specifically promotes assembly at the plus-end. J Cell Biol. 1987; 105:2203–2215. [PubMed: 2890645]
3. Brouhard GJ, et al. XMAP215 is a processive microtubule polymerase. Cell. 2008; 132:79–88. [PubMed: 18191222]

4. Kronja I, Kruljac-Letunic A, Caudron-Herger M, Bieling P, Karsenti E. XMAP215-EB1 interaction is required for proper spindle assembly and chromosome segregation in Xenopus egg extract. Molecular biology of the cell. 2009; 20:2684–2696. [PubMed: 19369422]
5. Reber SB, et al. XMAP215 activity sets spindle length by controlling the total mass of spindle microtubules. Nature cell biology. 2013; 15:1116–1122. [PubMed: 23974040]
6. Gergely F, Draviam VM, Raff JW. The ch-TOG/XMAP215 protein is essential for spindle pole organization in human somatic cells. Genes Dev. 2003; 17:336–341. [PubMed: 12569123]
7. Cassimeris L, Morabito J. TOGp, the human homolog of XMAP215/Dis1, is required for centrosome integrity, spindle pole organization, and bipolar spindle assembly. Molecular biology of the cell. 2004; 15:1580–1590. [PubMed: 14718566]
8. Heald R, et al. Self-organization of microtubules into bipolar spindles around artificial chromosomes in Xenopus egg extracts. Nature. 1996; 382:420–425. [PubMed: 8684481]
9. Carazo-Salas RE, et al. Generation of GTP-bound Ran by RCC1 is required for chromatin-induced mitotic spindle formation. Nature. 1999; 400:178–181. [PubMed: 10408446]
10. Ohba T, Nakamura M, Nishitani H, Nishimoto T. Self-organization of microtubule asters induced in Xenopus egg extracts by GTP-bound Ran. Science. 1999; 284:1356–1358. [PubMed: 10334990]
11. Kalab P, Pu RT, Dasso M. The ran GTPase regulates mitotic spindle assembly. Curr Biol. 1999; 9:481–484. [PubMed: 10322113]
12. Wilde A, Zheng Y. Stimulation of microtubule aster formation and spindle assembly by the small GTPase Ran. Science. 1999; 284:1359–1362. [PubMed: 10334991]
13. Kalab P, Weis K, Heald R. Visualization of a Ran-GTP gradient in interphase and mitotic Xenopus egg extracts. Science. 2002; 295:2452–2456. [PubMed: 11923538]
14. Kalab P, Pralle A, Isacoff EY, Heald R, Weis K. Analysis of a RanGTP-regulated gradient in mitotic somatic cells. Nature. 2006; 440:697–701. [PubMed: 16572176]
15. Caudron M, Bunt G, Bastiaens P, Karsenti E. Spatial coordination of spindle assembly by chromosome-mediated signaling gradients. Science. 2005; 309:1373–1376. [PubMed: 16123300]
16. Goshima G, Mayer M, Zhang N, Stuurman N, Vale RD. Augmin: a protein complex required for centrosome-independent microtubule generation within the spindle. J Cell Biol. 2008; 181:421–429. [PubMed: 18443220]
17. Petry S, Groen AC, Ishihara K, Mitchison TJ, Vale RD. Branching microtubule nucleation in Xenopus egg extracts mediated by augmin and TPX2. Cell. 2013; 152:768–777. [PubMed: 23415226]
18. Wittmann T, Wilm M, Karsenti E, Vernos I. TPX2, A novel xenopus MAP involved in spindle pole organization. J Cell Biol. 2000; 149:1405–1418. [PubMed: 10871281]
19. Gruss OJ, et al. Ran induces spindle assembly by reversing the inhibitory effect of importin alpha on TPX2 activity. Cell. 2001; 104:83–93. [PubMed: 11163242]
20. Gruss OJ, et al. Chromosome-induced microtubule assembly mediated by TPX2 is required for spindle formation in HeLa cells. Nature cell biology. 2002; 4:871–879. [PubMed: 12389033]
21. Aguirre-Portoles C, et al. Tpx2 controls spindle integrity, genome stability, and tumor development. Cancer Res. 2012; 72:1518–1528. [PubMed: 22266221]
22. Perez de Castro I, Malumbres M. Mitotic Stress and Chromosomal Instability in Cancer: The Case for TPX2. Genes Cancer. 2012; 3:721–730. [PubMed: 23634259]
23. Schatz CA, et al. Importin alpha-regulated nucleation of microtubules by TPX2. EMBO J. 2003; 22:2060–2070. [PubMed: 12727873]
24. Giesecke A, Stewart M. Novel binding of the mitotic regulator TPX2 (target protein for Xenopus kinesin-like protein 2) to importin-alpha. J Biol Chem. 2010; 285:17628–17635. [PubMed: 20335181]
25. Trieselmann N, Armstrong S, Rauw J, Wilde A. Ran modulates spindle assembly by regulating a subset of TPX2 and Kid activities including Aurora A activation. J Cell Sci. 2003; 116:4791–4798. [PubMed: 14600264]

26. Brunet S, et al. Characterization of the TPX2 domains involved in microtubule nucleation and spindle assembly in Xenopus egg extracts. Molecular biology of the cell. 2004; 15:5318–5328. [PubMed: 15385625]
27. Tanenbaum ME, et al. Kif15 cooperates with eg5 to promote bipolar spindle assembly. Curr Biol. 2009; 19:1703–1711. [PubMed: 19818618]
28. Vanneste D, Takagi M, Imamoto N, Vernos I. The role of Hklp2 in the stabilization and maintenance of spindle bipolarity. Curr Biol. 2009; 19:1712–1717. [PubMed: 19818619]
29. Koffa MD, et al. HURP is part of a Ran-dependent complex involved in spindle formation. Curr Biol. 2006; 16:743–754. [PubMed: 16631581]
30. Wittmann T, Boleti H, Antony C, Karsenti E, Vernos I. Localization of the kinesin-like protein Xklp2 to spindle poles requires a leucine zipper, a microtubule-associated protein, and dynein. J Cell Biol. 1998; 143:673–685. [PubMed: 9813089]
31. Ma N, Titus J, Gable A, Ross JL, Wadsworth P. TPX2 regulates the localization and activity of Eg5 in the mammalian mitotic spindle. J Cell Biol. 2011; 195:87–98. [PubMed: 21969468]
32. Helmke KJ, Heald R. TPX2 levels modulate meiotic spindle size and architecture in Xenopus egg extracts. J Cell Biol. 2014; 206:385–393. [PubMed: 25070954]
33. Tsai MY, et al. A Ran signalling pathway mediated by the mitotic kinase Aurora A in spindle assembly. Nature cell biology. 2003; 5:242–248. [PubMed: 12577065]
34. Bayliss R, Sardon T, Vernos I, Conti E. Structural basis of Aurora-A activation by TPX2 at the mitotic spindle. Mol Cell. 2003; 12:851–862. [PubMed: 14580337]
35. Kufer TA, et al. Human TPX2 is required for targeting Aurora-A kinase to the spindle. J Cell Biol. 2002; 158:617–623. [PubMed: 12177045]
36. Brunet S, et al. Meiotic regulation of TPX2 protein levels governs cell cycle progression in mouse oocytes. PLoS One. 2008; 3:e3338. [PubMed: 18833336]
37. Groen AC, Maresca TJ, Gatlin JC, Salmon ED, Mitchison TJ. Functional overlap of microtubule assembly factors in chromatin-promoted spindle assembly. Molecular biology of the cell. 2009; 20:2766–2773. [PubMed: 19369413]
38. Bird AW, Hyman AA. Building a spindle of the correct length in human cells requires the interaction between TPX2 and Aurora A. J Cell Biol. 2008; 182:289–300. [PubMed: 18663142]
39. Scrofani J, Sardon T, Meunier S, Vernos I. Microtubule nucleation in mitosis by a RanGTP-dependent protein complex. Curr Biol. 2015; 25:131–140. [PubMed: 25532896]
40. Kollman JM, Merdes A, Mourey L, Agard DA. Microtubule nucleation by gamma-tubulin complexes. Nat Rev Mol Cell Biol. 2011; 12:709–721. [PubMed: 21993292]
41. Bieling P, Telley IA, Hentrich C, Piehler J, Surrey T. Fluorescence microscopy assays on chemically functionalized surfaces for quantitative imaging of microtubule, motor, and +TIP dynamics. Methods Cell Biol. 2010; 95:555–580. [PubMed: 20466153]
42. Al-Bassam J, et al. Fission yeast Alp14 is a dose-dependent plus end-tracking microtubule polymerase. Molecular biology of the cell. 2012; 23:2878–2890. [PubMed: 22696680]
43. Podolski M, Mahamdeh M, Howard J. Stu2, the budding yeast XMAP215/Dis1 homolog, promotes assembly of yeast microtubules by increasing growth rate and decreasing catastrophe frequency. J Biol Chem. 2014; 289:28087–28093. [PubMed: 25172511]
44. Li W, et al. EB1 promotes microtubule dynamics by recruiting Sentin in Drosophila cells. J Cell Biol. 2011; 193:973–983. [PubMed: 21646401]
45. Wieczorek M, Bechstedt S, Chaaban S, Brouhard GJ. Microtubule-associated proteins control the kinetics of microtubule nucleation. Nature cell biology. 2015; 17:907–916. [PubMed: 26098575]
46. Bieling P, et al. CLIP-170 tracks growing microtubule ends by dynamically recognizing composite EB1/tubulin-binding sites. J Cell Biol. 2008; 183:1223–1233. [PubMed: 19103809]
47. Bieling P, et al. Reconstitution of a microtubule plus-end tracking system in vitro. Nature. 2007; 450:1100–1105. [PubMed: 18059460]
48. Maurer SP, et al. EB1 accelerates two conformational transitions important for microtubule maturation and dynamics. Curr Biol. 2014; 24:372–384. [PubMed: 24508171]
49. Chretien D, Fuller SD, Karsenti E. Structure of growing microtubule ends: two-dimensional sheets close into tubes at variable rates. J Cell Biol. 1995; 129:1311–1328. [PubMed: 7775577]

50. Maurer SP, Bieling P, Cope J, Hoenger A, Surrey T. GTPgammaS microtubules mimic the growing microtubule end structure recognized by end-binding proteins (EBs). Proc Natl Acad Sci U S A. 2011; 108:3988–3993. [PubMed: 21368119]
51. Ghosh S, Hentrich C, Surrey T. Micropattern-controlled local microtubule nucleation, transport, and mesoscale organization. ACS Chem Biol. 2013; 8:673–678. [PubMed: 23294267]
52. Voter WA, Erickson HP. The kinetics of microtubule assembly. Evidence for a two-stage nucleation mechanism. J Biol Chem. 1984; 259:10430–10438. [PubMed: 6469971]
53. Wang HW, Long S, Finley KR, Nogales E. Assembly of GMPCPP-bound tubulin into helical ribbons and tubes and effect of colchicine. Cell Cycle. 2005; 4:1157–1160. [PubMed: 16123589]
54. Mozziconacci J, Sandblad L, Wachsmuth M, Brunner D, Karsenti E. Tubulin dimers oligomerize before their incorporation into microtubules. PLoS One. 2008; 3:e3821. [PubMed: 19043587]
55. van Breugel M, Drechsel D, Hyman A. Stu2p, the budding yeast member of the conserved Dis1/XMAP215 family of microtubule-associated proteins is a plus end-binding microtubule destabilizer. J Cell Biol. 2003; 161:359–369. [PubMed: 12719475]
56. Hyman AA, Salser S, Drechsel DN, Unwin N, Mitchison TJ. Role of GTP hydrolysis in microtubule dynamics: information from a slowly hydrolyzable analogue, GMPCPP. Molecular biology of the cell. 1992; 3:1155–1167. [PubMed: 1421572]
57. Hyman AA, Chretien D, Arnal I, Wade RH. Structural changes accompanying GTP hydrolysis in microtubules: information from a slowly hydrolyzable analogue guanylyl-(alpha,beta)-methylene-diphosphonate. J Cell Biol. 1995; 128:117–125. [PubMed: 7822409]
58. Alushin GM, et al. High-resolution microtubule structures reveal the structural transitions in alphabeta-tubulin upon GTP hydrolysis. Cell. 2014; 157:1117–1129. [PubMed: 24855948]
59. Bechstedt S, Lu K, Brouhard GJ. Doublecortin recognizes the longitudinal curvature of the microtubule end and lattice. Curr Biol. 2014; 24:2366–2375. [PubMed: 25283777]
60. Ayaz P, Ye X, Huddleston P, Brautigam CA, Rice LM. A TOG:alphabeta-tubulin complex structure reveals conformation-based mechanisms for a microtubule polymerase. Science. 2012; 337:857–860. [PubMed: 22904013]
61. Coombes CE, Yamamoto A, Kenzie MR, Odde DJ, Gardner MK. Evolving tip structures can explain age-dependent microtubule catastrophe. Curr Biol. 2013; 23:1342–1348. [PubMed: 23831290]
62. Tsai MY, Zheng Y. Aurora A kinase-coated beads function as microtubule-organizing centers and enhance RanGTP-induced spindle assembly. Curr Biol. 2005; 15:2156–2163. [PubMed: 16332542]
63. Zacharias DA, Violin JD, Newton AC, Tsien RY. Partitioning of lipid-modified monomeric GFPs into membrane microdomains of live cells. Science. 2002; 296:913–916. [PubMed: 11988576]
64. Snapp EL, et al. Formation of stacked ER cisternae by low affinity protein interactions. J Cell Biol. 2003; 163:257–269. [PubMed: 14581454]
65. Duellberg C, et al. Reconstitution of a hierarchical +TIP interaction network controlling microtubule end tracking of dynein. Nature cell biology. 2014; 16:804–811. [PubMed: 24997520]
66. Castoldi M, Popov AV. Purification of brain tubulin through two cycles of polymerization-depolymerization in a high-molarity buffer. Protein Expr Purif. 2003; 32:83–88. [PubMed: 14680943]
67. Hyman A, et al. Preparation of modified tubulins. Methods Enzymol. 1991; 196:478–485. [PubMed: 2034137]

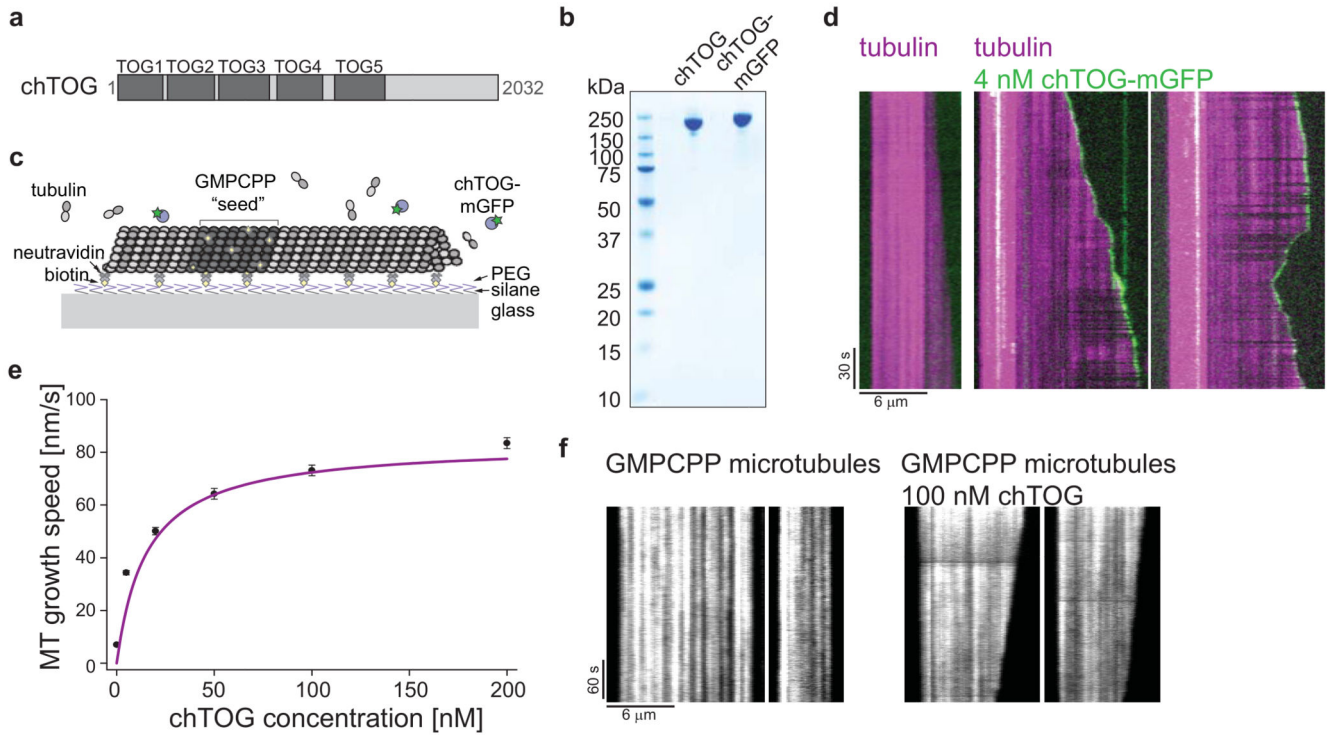

Figure 1. Human chTOG is a microtubule polymerase

(a) Scheme illustrating the domain structure of human chTOG. **(b)** Coomassie Blue-stained SDS-PAGE gel showing 1 µg of purified recombinant chTOG constructs. **(c)** Scheme of the experimental setup. **(d)** Dual colour TIRF microscopy kymographs showing Atto647N-labelled microtubules (magenta) growing in the absence or presence of 4 nM full-length chTOG-mGFP (green). **(e)** Plot of the mean growth speed as a function of the chTOG concentration. Data points, black; error bars are SEM; Hyperbolic fit (one-site binding) - magenta curve. Number of 25 s-growth intervals used to measure individual velocities for each chTOG concentration: 0 nM – 1,003; 5 nM – 966; 20 nM – 661; 50 nM – 499; 100 nM – 510; 200 nM – 600. Atto647N-labelled tubulin concentration in **(d)** and **(e)** was 7.5 µM. Data were pooled from two datasets. **(f)** Kymographs showing GMPCPP-stabilised Atto647N-labelled microtubules in the absence of soluble tubulin and either in the absence (left) or presence (right) of 100 nM chTOG. Scale bars as indicated.

Europe PMC Funders Author Manuscripts

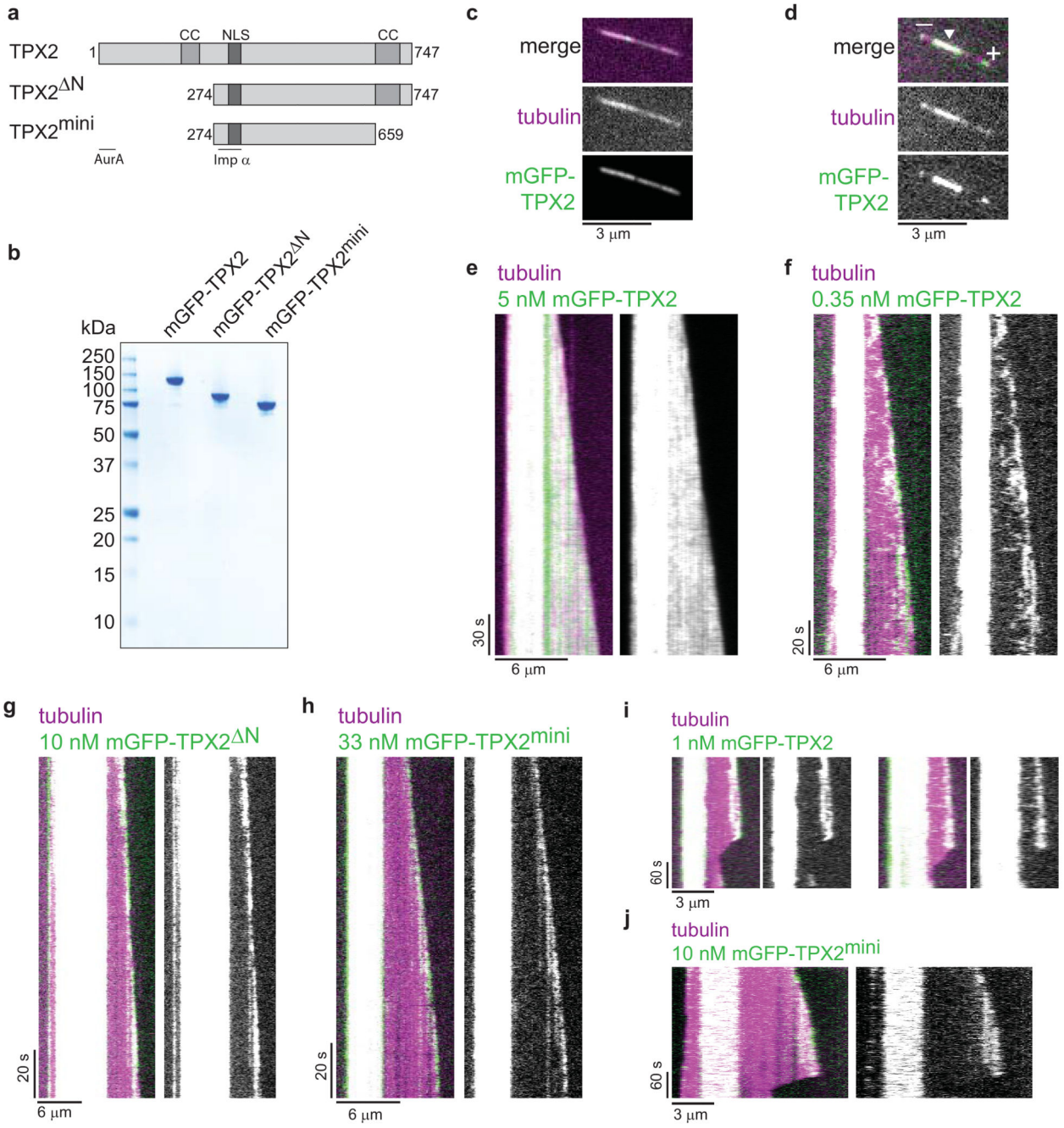

Figure 2. The central part of human TPX2 determines its binding preference for growing microtubule ends

(a) Scheme of the human TPX2 constructs used in this study: full-length TPX2, N-terminally truncated TPX2 containing amino acids 274 - 747 ($TPX2^{\Delta N}$), and a minimal TPX2 construct containing amino acids 274 - 659 ($TPX2^{mini}$). Regions known to interact with Aurora A (AurA), importin α (Imp α) are indicated, together with predicted coil coils (CC) and nuclear localisation signal (NLS). **(b)** Coomassie Blue-stained SDS-PAGE gel showing 1 μg of purified recombinant TPX2 constructs. **(c, d)** Single channel and merged

Europe PMC Funders Author Manuscripts

TIRF microscopy images showing how mGFP-TPX2 (green in merge) at 5 nM **(c)** and 0.35 nM **(d)** binds either all along **(c)** or preferentially to the growing ends and the GMPCPP segment **(d)** of a growing Atto647N-labelled microtubule (magenta in merge) ("−" and "+" indicate end binding, the GMPCPP "seed" is marked by an arrowhead). **(e)** Kymographs depicting the time course of binding of 5 nM mGFP-TPX2 all along a growing microtubule. Att647N-labelled tubulin concentration was 7.5 μM. **(f)** Kymographs depicting the time course of 0.35 nM mGFP-TPX2 binding to a growing microtubule end and the GMPCPP "seed". Att647N-labelled tubulin concentration was 12.5 μM. **(g, h)** Kymographs showing binding of **(g)** 10 nM mGFP-TPX2$^{\Delta N}$ and **(h)** 33 nM mGFP-TPX2^{mini} to dynamic microtubules (merged channels on the left, mGFP-TPX2 on the right). Atto647N-labelled tubulin concentration is 12.5 and 15 μM, respectively. **(i, j)** Kymographs showing that neither **(i)** 1 nM full-length mGFP-TPX2 nor **(j)** 10 nM TPX2^{mini} binds to shrinking microtubules. Atto647N-labelled tubulin concentrations were 5 μM and 7.5 μM, respectively. For all kymograph pairs: merged channel - left, mGFP-TPX2 channel - right. Scale bars as indicated.

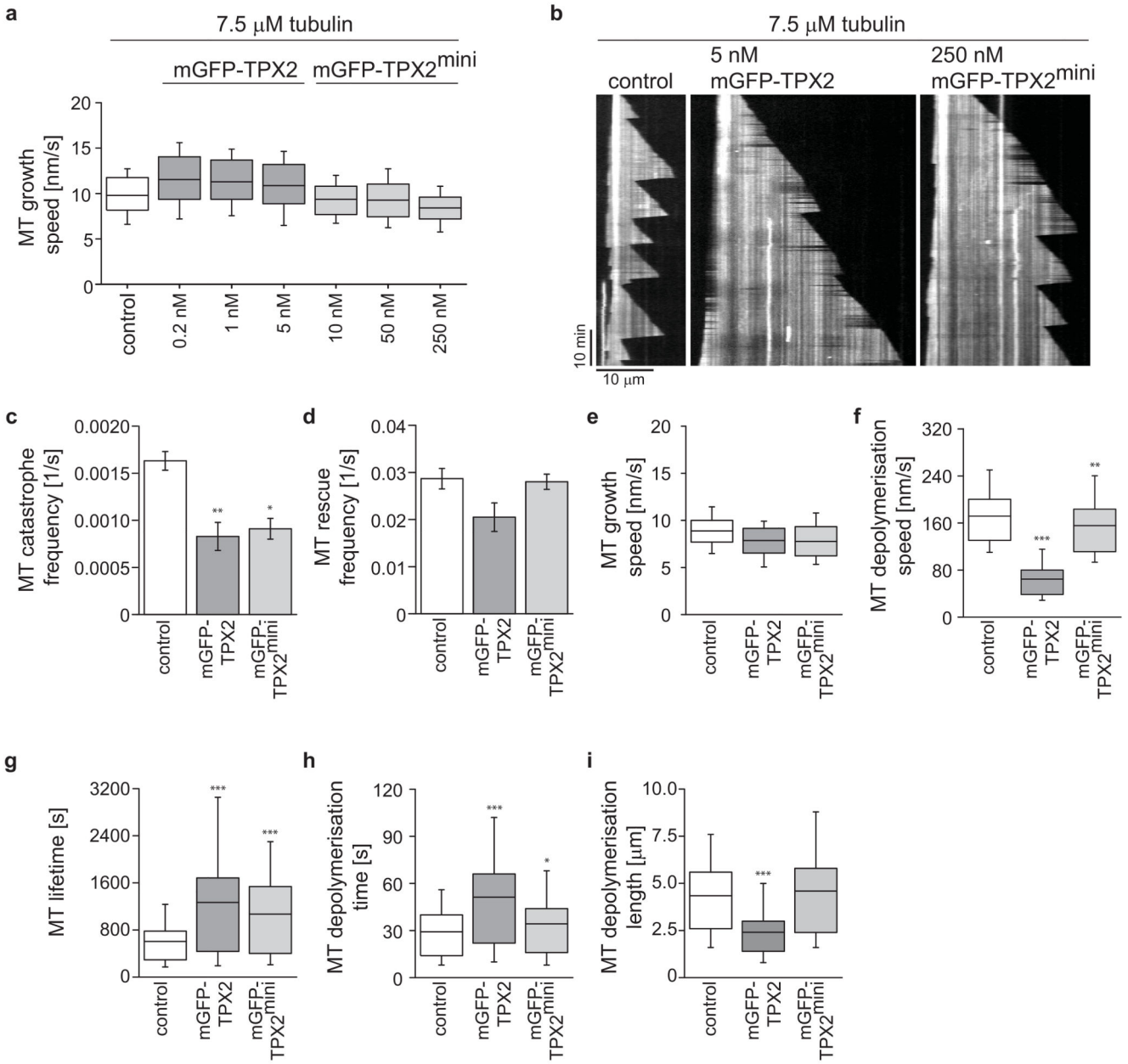

Figure 3. Effect of full-length TPX2 and TPX2^{mini} on microtubule dynamic instability parameters

(a) Modified box-and-whiskers graph for the microtubule growth speeds in the absence (control) and presence of different concentrations of full-length mGFP-TPX2 and mGFP-TPX2^{mini}, as indicated. Number of observed microtubule growth episodes per condition: control – n=150; mGFP-TPX2: 0.2 nM – n= 160, 1 nM – n=150, 5 nM – n=114; mGFP-TPX2^{mini}: 10 nM – n=153, 50 nM – n=121, 250 nM – n=154. All events are from one dataset each. **(b)** TIRF microscopy kymographs showing dynamic Atto647N-labelled microtubules in the absence (control) or presence of 5 nM mGFP-TPX2 or 250 nM mGFP-TPX2^{mini}. Scale bars as indicated. Bar graphs showing microtubule **(c)** catastrophe and **(d)**

rescue frequencies, and box-and-whiskers graphs showing microtubule **(e)** growth and **(f)** depolymerisation speeds, for control, 5 nM mGFP-TPX2, and 250 nM mGFP-TPX2^{mini}, as indicated. Box-and-whiskers graphs show **(g)** microtubule lifetimes, **(h)** depolymerisation times and **(i)** depolymerisation lengths for the same conditions. Data for (c-i) were pooled from three datasets each. Total number of analysed events per condition: (c) catastrophes (total growth time in brackets): control – n=757 (457,280 s), mGFP-TPX2 –n= 209 (267,644 s), mGFP-TPX2^{mini} – n=385 (409,675 s); (d) rescues (total depolymerisation time in brackets): control – n=612 (22,062 s), mGFP-TPX2 – n=209 (10,708 s), mGFP-TPX2^{mini} – n=376 (13,130 s); (e) growth episodes: control – n=863, 5 nM mGFP-TPX2 – n=271, 250 nM mGFP-TPX2^{mini} –n=477; (f) depolymerisation episodes: control – n=756, 5 nM, mGFP-TPX2 – n=211, 250 nM mGFP-TPX2^{mini} –n=383. The same data were used in (g)-(i) (see Supplementary Note). Atto647N-labelled tubulin concentration was always 7.5 μM. Errors in bar graphs are SEM. For the modified box-and-whiskers plots the boxes range from 25th to 75th percentile, the whiskers span from 10th to 90th percentile, the horizontal line marks the mean value. * $p \leq 0.05$; ** $p \leq 0.01$; *** $p \leq 0.001$ (only displayed for comparisons with control); determined for the comparison of mean values analysing raw data (Tukey's test in conjunction with One Way ANOVA).

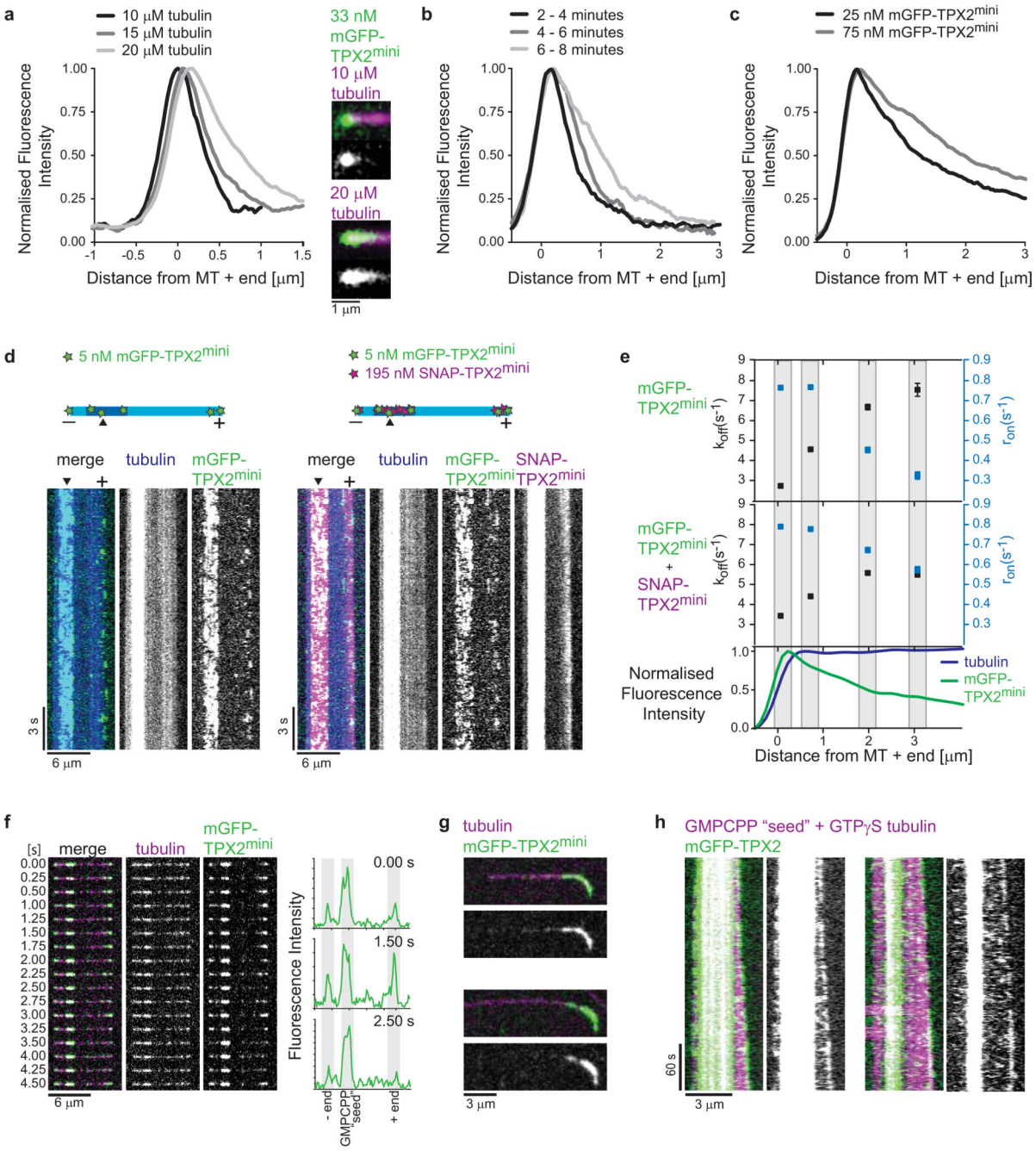

Figure 4. TPX2 binds to a unique binding region at growing microtubule ends

(a) Right: Images of 33 nM mGFP-TPX2^{mini} (green in merge) at growing Atto647N-labelled microtubule ends (magenta in merge) at the indicated tubulin concentrations. Left: Averaged mGFP-TPX2^{mini} intensity profiles at the end regions of microtubules growing in the presence of 33 nM mGFP-TPX2^{mini} and the indicated Atto647N-labelled tubulin concentrations. **(b)** Averaged mGFP-TPX2^{mini} intensity profiles at the end regions of microtubules growing in the presence of 33 nM mGFP-TPX2^{mini} and 20 μM Atto647N-labelled tubulin for three different time windows after start of growth. **(c)** Averaged mGFP-

Europe PMC Funders Author Manuscripts

Europe PMC Funders Author Manuscripts

TPX2^{mini} intensity profiles for the indicated mGFP-TPX2^{mini} concentrations at 25 μM Atto647N-labelled tubulin. **(d)** Cartoons depicting the assay conditions and TIRF microscopy kymographs showing single molecule binding events of 5 nM mGFP-TPX2^{mini} (green in merge) to the ends of growing Atto565-labelled microtubules (blue in merge) in the absence or presence of 195 nM Alexa647-labelled SNAP-TPX2^{mini} (magenta in merge). **(e)** Dissociation rate constant k_{off} and association rate r_{on}, respectively, as determined for the conditions in (d) from the dwell and waiting time distributions of the single mGFP-TPX2^{mini} molecule binding and unbinding events (Supplementary Fig. 3a-c, Supplementary Note) as a function of the distance from the growing microtubule plus end. Note that the increase in k_{off} values and decrease in r_{on} values is less steep in the presence of excess Alexa647-labelled SNAP-TPX2^{mini}, agreeing with (4c). Lower panel: The normalised total fluorescence intensity of all mGFP-TPX2^{mini} binding events shows their steady state distribution. **(f)** Kymographs and instantaneous intensity line scans at different times, as indicated, showing strong temporal fluctuations of the fluorescence intensity of mGFP-TPX2^{mini} (25 nM, green in merge) at growing Atto647N-labelled microtubule ends (magenta in merge, 12.5 μM tubulin). **(g)** TIRF microscopy images showing 33 nM mGFP-TPX2^{mini} (green in merge, lower panels) accumulating strongly at the curved microtubule ends of Atto647N-labelled growing microtubules (magenta in merge, 30 μM tubulin). **(h)** Kymographs of 5 nM mGFP-TPX2 (green in merge) localising to the ends of Atto647N-labelled microtubules (magenta in merge, 25 μM tubulin) growing in the presence of the slowly-hydrolysable GTP analogue GTPγS. Scale bars as indicated.

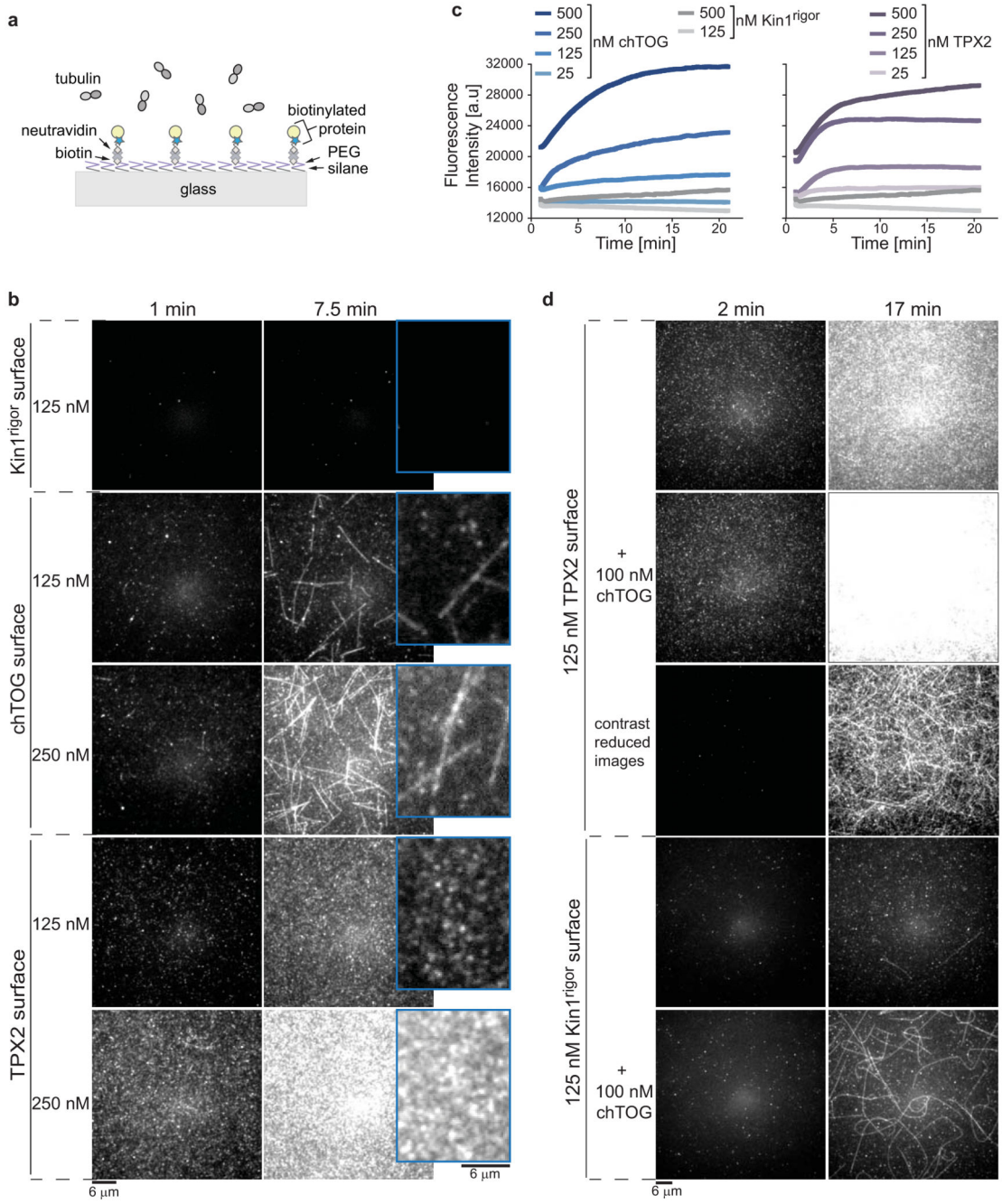

Figure 5. Surface-immobilised TPX2 arrests nucleation intermediates, but in combination with chTOG efficiently nucleates microtubules

(a) Scheme of the experimental setup for the 'surface' nucleation assay. **(b)** TIRF microscopy images from a time series showing Atto647N-labelled microtubules and/or tubulin particles on a glass surface with immobilised biotinylated Kin1^{rigor} mutant, chTOG or TPX2 after pre-incubation at the indicated concentrations. Insets on the right depict magnified images of the same surface at 7.5 min. **(c)** Time courses of the mean Atto647N-tubulin fluorescence intensities measured at the surface for the entire field of view for

different chTOG, TPX2 and Kin1^{rigor} densities. Concentrations of biotinylated proteins used for surface incubation as indicated. The same Kin1^{rigor} curve is shown as a control for both chTOG and TPX2 plots. Note that the fluorescence signal typically represents the sum of several different tubulin species: soluble tubulin in the TIRF field (creating part of the background), immobilised individual tubulins (e.g. bound to chTOG), tubulin 'stubs' (bound to TPX2) and microtubules (bound to chTOG or TPX2). Raw intensities including background are shown. **(d)** Time series of TIRF microscopy images showing nucleation and growth of Atto647N-labelled microtubules on surfaces with immobilised biotinylated TPX2 (pre-incubated at 125 nM, top three rows) or, for controls, with a biotinylated Kin1^{rigor} (pre-incubated at 125 nM, bottom two rows) in either the absence or presence of 100 nM untagged chTOG, as indicated. Because of the high microtubule density at the TPX2 surface in the presence of chTOG, the same time series is also shown with reduced contrast for better visualisation of individual microtubules. Atto647N-labelled tubulin concentration was always 12.5 μM. Scale bars as indicated. t = 0 when the sample is placed at 30°C.

Europe PMC Funders Author Manuscripts

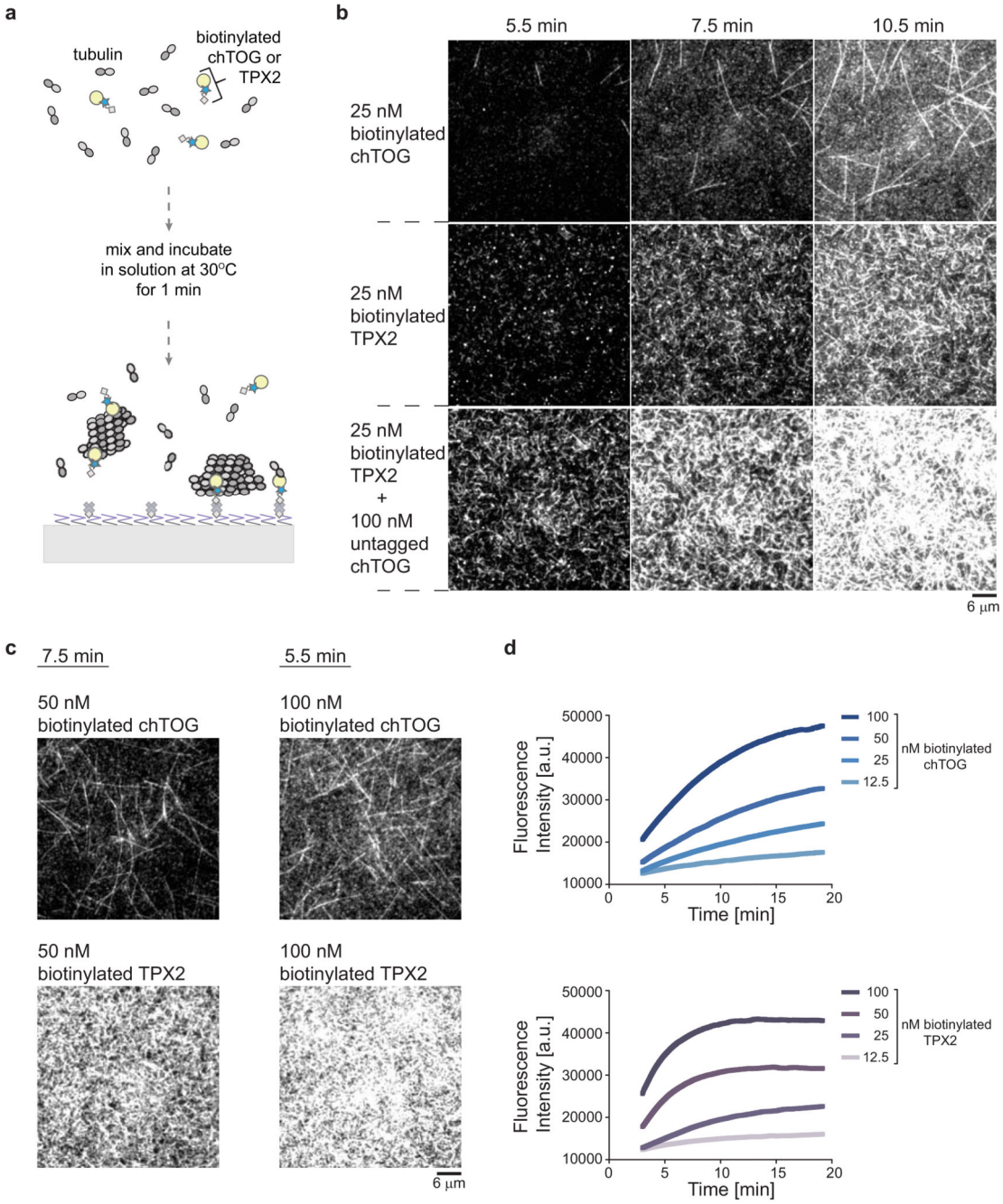

Figure 6. In solution TPX2 nucleates microtubules more efficiently than chTOG

(a) Scheme of the experimental setup for the 'solution' nucleation assay. **(b)** Time series of TIRF microscopy images showing Atto647N-labelled microtubules that nucleated in solution in the presence of nucleation factors as indicated, followed after 1 min by binding to a neutravidin-coated surface via the biotinylated protein present as indicated. **(c)** TIRF microscopy images showing examples the concentration dependent nucleation efficiencies of chTOG- and TPX2-mediated microtubule nucleation in the 'solution' nucleation assay. **(d)** Time courses of mean Atto647N-tubulin fluorescence intensities measured for the entire

field of view in ‘solution’ at the biotinylated chTOG and TPX2 concentrations as indicated. Note that the fluorescence signal typically represents the sum of several different tubulin species (see note in legend of Fig. 5c). Raw intensities including background are shown. Atto647N-labelled tubulin concentration was always 12.5 μM. Other protein concentrations and scale bar as indicated. t = 0 when the sample is placed at 30°C.

Europe PMC Funders Author Manuscripts

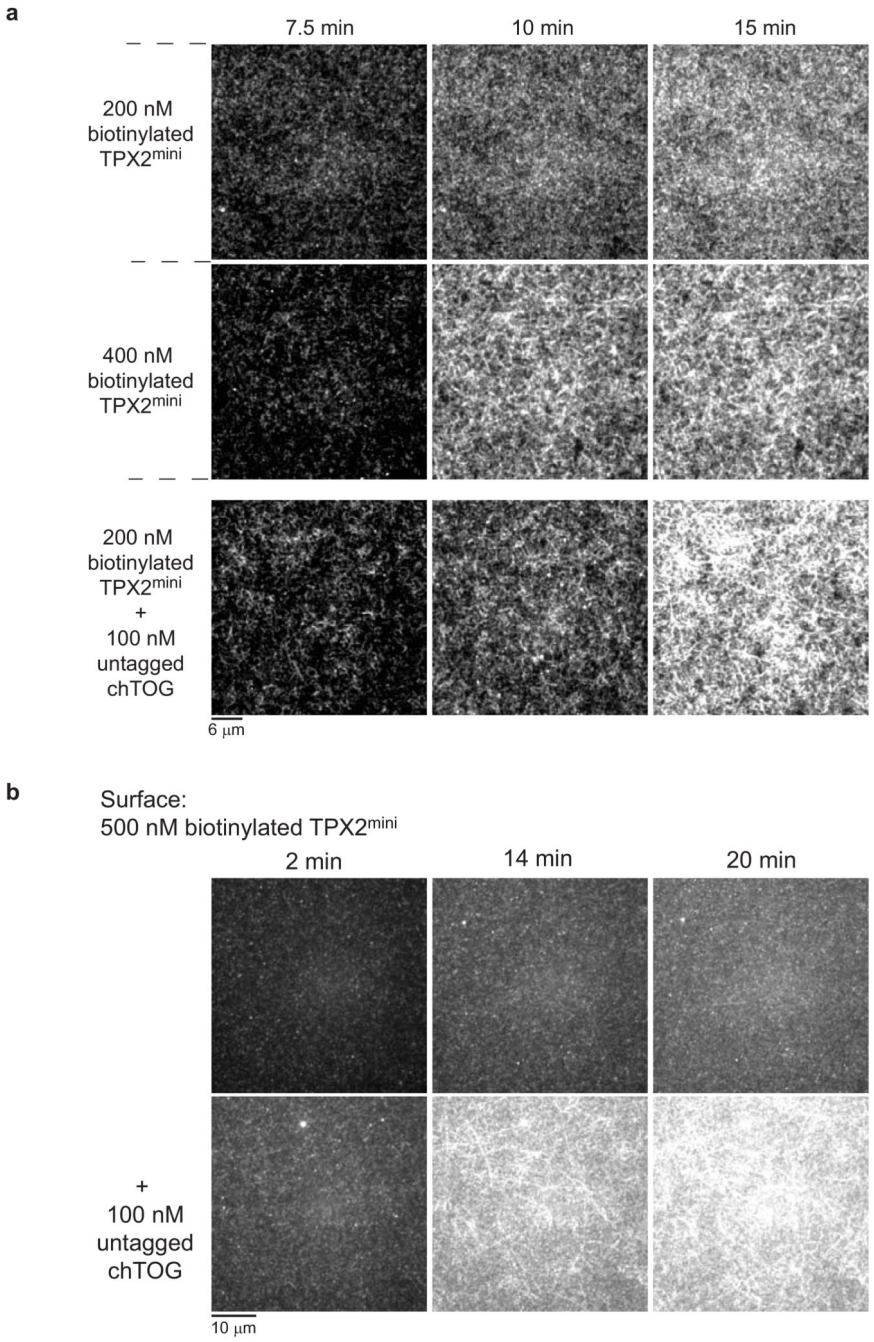

Figure 7. The central region of TPX2 is sufficient to stimulate microtubule nucleation

(a) Times series of TIRF microscopy images of the 'solution' nucleation assay where microtubules that nucleated in solution in the presence of different concentrations of biotinylated TPX2^{mini} and in the additional presence of untagged chTOG, followed after 1 min by binding to a neutravidin-coated surface. **(b)** Time series of TIRF microscopy images of the 'surface' nucleation experiments with immobilised biotinylated TPX2^{mini} (pre-incubated at 500 nM) in the absence (top row) or presence (bottom row) of untagged

Europe PMC Funders Author Manuscripts

chTOG. Atto647N-labelled tubulin concentration was always 12.5 μM. Other protein concentrations and scale bars as indicated. t = 0 when the sample is placed at 30°C.

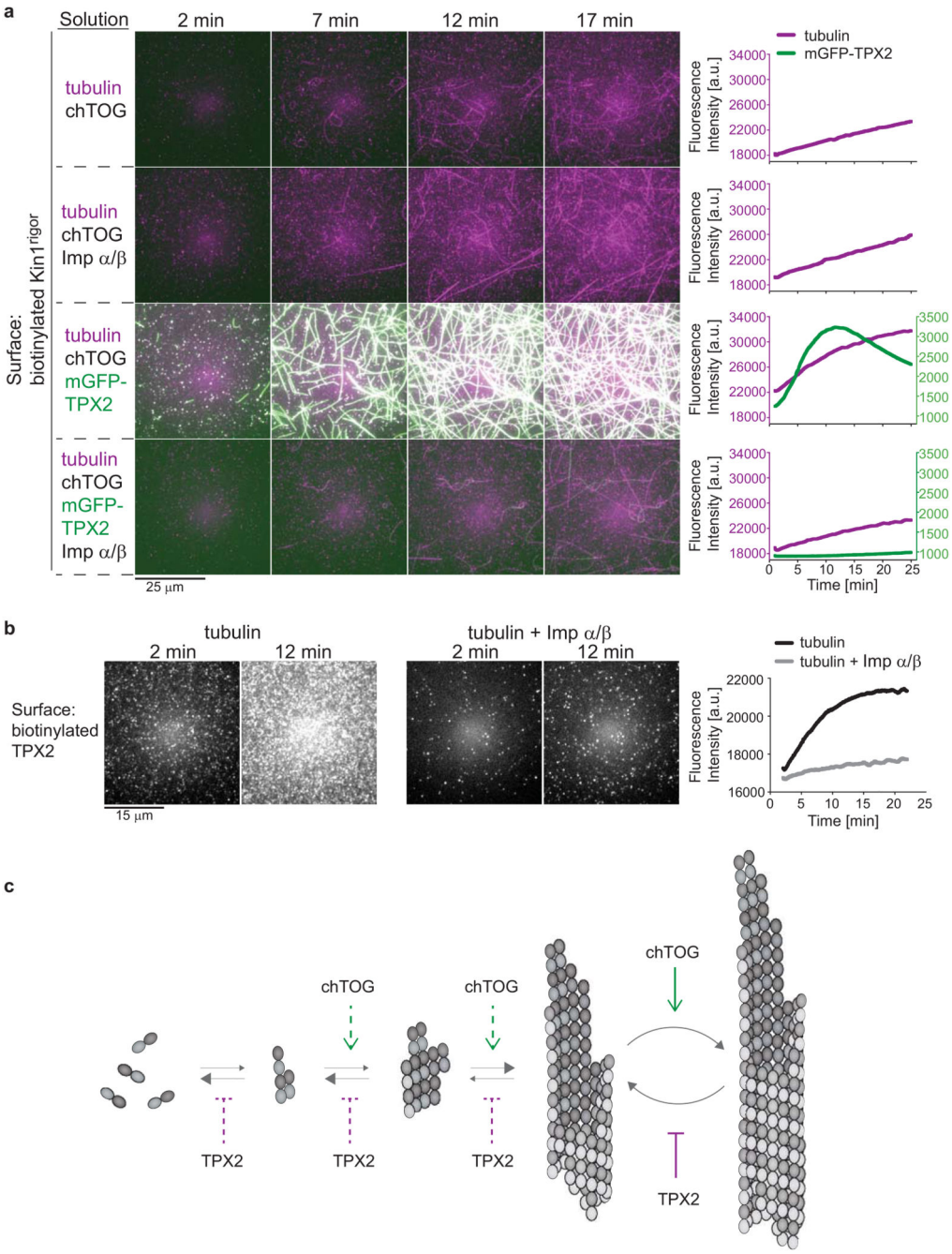

Figure 8. Regulation of TPX2 and chTOG-stimulated microtubule nucleation by importins

(a) Time series of TIRF microscopy images showing microtubule nucleation and growth on surfaces with immobilised biotinylated rigor kinesin (pre-incubated at 125 nM) always in the presence of 100 nM chTOG and Atto647N-labelled tubulin, without and with additional 500 nM importin α/β complex (first and second row, respectively), 100 nM mGFP-TPX2 (third row) or both 500 nM importin α/β and 100 nM mGFP-TPX2 (fourth row) as indicated. Plots showing the time course of the mean Atto647N-labelled microtubule (magenta) and mGFP-TPX2 (green) intensities for the same experiments are shown next to each individual times

series of images. Note that the mGFP-TPX2 signal declines at later time points likely due to depletion of TPX2 from solution due to binding to the efficiently nucleated growing microtubules. **(b)** Time series of TIRF microscopy images showing that compared to a control (left), inclusion of importin α/β (500 nM) inhibits stabilisation of Atto647N-labelled nucleation intermediates by surface-immobilised biotinylated TPX2 (pre-incubated at 125 nM) (right image pair). Plot showing the time course of the mean Atto647N-labelled tubulin intensities on the surface (right). Atto647N-labelled tubulin concentration was always 12.5 μM. Scale bars as indicated. t = 0 when the sample is placed at 30°C. **(c)** Model of synergistic TPX2 and chTOG-stimulated microtubule nucleation and growth. Different reactions, all promoting nucleation and growth, are regulated by the distinct and complementary activities of TPX2 and chTOG.